Development of catalysts for possible application in the conversion of xylose to xylitol,

by

Shivek Rajkumar

Submitted in fulfilment of the academic requirements of

Master of Science

In Engineering

Chemical Engineering

College of Agriculture, Engineering and Science

University of KwaZulu-Natal

Howard College

South Africa

Supervisor: Dr Bruce Sithole

17 October 2022

DECLARATION

I, Shivek Rajkumar, declare that

1. The research reported in this thesis, except where otherwise indicated, is original.

2. This thesis has not been submitted for any degree or examination at any other university.

3. This thesis does not contain other persons' data, pictures, graphs or other information unless specifically acknowledged as being sourced from other persons.

4. This thesis does not contain other persons' writing unless specifically acknowledged as being sourced from other researchers. Where other written sources have been quoted, then:

a. Their words have been rewritten, but the general information attributed to them has been referenced

b. Where their exact words have been used, then their writing has been placed in italics and inside quotation marks and referenced.

5. This thesis does not contain text, graphics or tables copied and pasted from the Internet, unless specifically acknowledged. The source is detailed in the thesis and the References sections.

Signed

……

As the candidate's Supervisor, I agree with the submission of this thesis

Signed

……

ABSTRACT

This project aimed to synthesize and characterize a novel catalyst for the transfer hydrogenation of xylose to xylitol.

A literature review revealed that palladium supported on an aluminium-tin mixed metal oxide support was the best catalyst to facilitate the reaction due to palladiums electron configuration, superior hydrogen bonding capacity, strong metal-support interactions and amphoteric nature of the support material.

Catalysts of nominal palladium loading 5 wt.% supported on tin-alumina mixed metal oxides of molar composition 10 %, 20 % ,30 %, 40 % and 50 % Sn were successfully synthesised using the microwave assisted sol-gel method and characterised using BET, EDX, SEM and XRD techniques.

Catalyst surface area decreased with tin composition from 200 m^2/g at 10% Sn to 60 $m^{2/}$g at 50% tin. SEM imaging confirmed nanoparticle formation with varying morphology depending on tin composition. EDX confirmed even dispersion of 5 wt. % Pd with one anomaly after impregnation and calcination. EDX maps indicate high density of Sn as it is more dense than Al. XRD confirmed the crystalline structure with the formation of both alpha and gamma-alumina phases.

A sustainability analysis indicated that the biological process is more environmentally friendly than the chemical route. Future work would entail testing the catalysts for their intended application.

ACKNOWLEDGMENTS

1. My Parents Reena and Roshan Rajkumar for their support

2. Dr Bruce Sithole for his supervision and support.

3. National Centre for Nanostructured Materials for providing the necessary facilities.

Contents

List of tables and figures

CHAPTER ONE: INTRODUCTION

1.1) Project scope

Value creation through recycling of by-products such as sawdust from the sawmilling industry has potential for job creation which has the added benefit f reducing waste in landfill sites.

Bio-refinery technologies aim to extract new value chains from biomass waste by extracting 99 % value from trees. This project aims to design, synthesise and characterize a novel catalyst, which improves on older technology such as base metal catalysts like nickel for upgrading xylose to xylitol.

The value of xylitol lies in its application as an industrial sweetening agent and its benefits over sucrose-based sugar and high fructose corn syrup. Classified as a sugar alcohol xylitol maintains a similar sweetness index to that of regular fructose and sucrose based sugar, contains 40 % fewer calories and exhibits a 90 % reduction in glycaemic index. Upon consumption, no blood sugar or insulin level spikes make it an attractive alternative for people with diabetes. Markets reports indicate that the global xylitol market size was 725.9 million USD in 2016, projecting over 1 billion USD by 2022 (Industry experts, 2017), making it an attractive research initiative to commercialise. A Secondary motivation for capitalising on this product includes the newly implemented legislation regarding sugar taxation in South Africa. The shortcomings of a nickel-based catalyst are low activity and stability. Low stability requires removal of leached nickel downstream via distillation to make the product fit for human consumption. Fermentation, albeit slower, has many advantages over the chemical route.

1.2 Aim and objectives

The project aim is to design, synthesise and characterize a suitable catalyst for the hydrogenation of xylose to xylitol. The objectives are three-fold:

1) Find an improvement on the chemical route, which initially used a nickel-based catalyst by completing a literature review of similar catalytic systems.
2) Use the literature review to identify drivers for a stable (leach resistant), highly active and selective catalyst for the hydrogenation of xylose to xylitol which will guide the design and synthesis by relating active structure to successful application results.
3) Characterize the synthesized catalyst.

1.3) Outline of the dissertation

Chapter 1: Introduction outlining research question.

Chapter 2: Literature review discussing research rational aligned with aims and objectives substantiated by work done by established researchers in the field, highlighting gaps to be addressed by this project.

Chapter3: Lists materials used with experimental methods implemented to achieve the desired outcomes.

Chapter 4: Presentation and discussion of the results obtained, including a sustainability analysis.

Chapter 5: Conclusions with recommendations for future work to improve research quality.

CHAPTER 2: LITERATURE REVIEW

This chapter compares different catalysts for biomass-derived platform chemical hydrogenations which will assist in the development of a catalyst for the transfer hydrogenation of xylose to xylitol as the systems analysed are similar in nature.

The alternate route for xylitol production is fermentation; a biological enzyme catalysed process compared to the chemical route. Due to deactivation and leaching, nickel catalysts cause product contamination. Furthermore, these catalysts require elevated temperatures and pressures. Using Pd can alleviate this burden, creating a competitive trade-off between initial capital expenditure, catalyst lifecycle and activity.

The active structure of the catalyst controlled during synthesis and post-treatment determines application performance. The differing support material of active Pd metal initiates differences in metal-support interaction, creating synergistic effects caused by different electronic, mechanical, and physicochemical effects in nature, modifying surface interaction with the substrate. The nature of certain supports result in bifunctional sites assisting reactions to proceed via alternate pathways, and the phenomenon of spillover effect promotes higher reaction rates by increasing the accessibility of the substrate and hydrogen to the active site.

2.1) Biomass feedstocks for hydrogenation

Trees are categorised commercially as soft and hardwoods, but this terminology cannot indicate the wood's hardness as overlap occurs in the average density of soft and hardwood. Classification by retention of leaves is also used, and the majority of commercial softwoods are evergreens (leaves are retained for many years) and Hardwood trees shed their leaves each Autumn (Yang and Jaakkola, 2011). Approximately two-thirds of wood comprises polysaccharides (cellulose and various hemicelluloses) (Alen, 1999). Cellulose is the fraction of the tree used in papermaking while the other components are discarded. The value extracted from trees increases by using the hemicellulose fraction as xylose from xylan polysaccharide hydrogenates to xylitol.

2.2) Metal selection using Sabatier's principle

Why Palladium?

Although adsorption is essential for catalysis to occur, it should not occur to the degree that adsorbed molecules are so tightly bound that they cannot desorb, blocking the active sites preventing further reaction limiting the number

of metals sites that are useful catalytic sites meeting this criterion of favourable adsorption strength (Atkins and Overton, no date)

Volcano relationship

A volcano relationship plot is depicted below where Pd is situated in the top area of the plot implying excellent capability of catalysing hydrogenation reactions (Liao, Lo and Tsang, 2015).

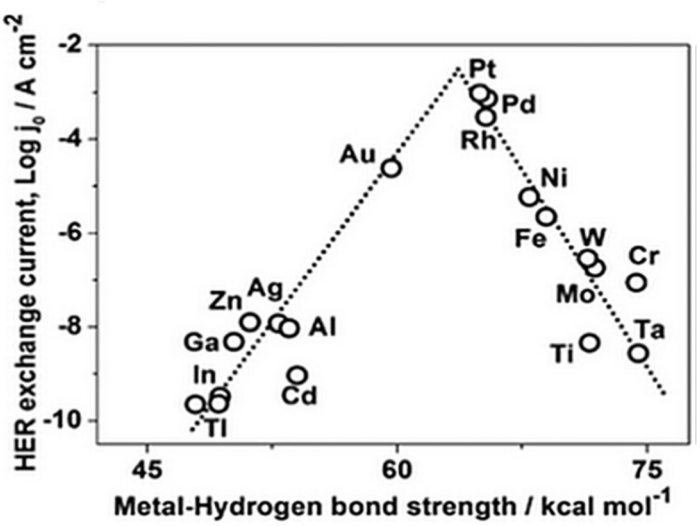

Figure 2.1:A volcano relationship of metal-hydrogen bond strength and activity of dissociating hydrogen/Hydrogen evolution reaction (Liao, Lo and Tsang, 2015)

According to Sabatier's principle, one of the oldest rules in catalysis adsorption energy should be neither too high nor too low, so the rate of adsorption should ideally be equal to the rate of desorption with equilibrium potential being as close to zero as possible so that the rate-limiting step is neither adsorption nor desorption. The above diagram is best interpreted in conjunction with a periodic table. The earlier d-block metals like titanium, chromium, molybdenum, tantalum and tungsten form very stable surface compounds due to their electronic configuration and valences characterised by higher metal-hydride bond strength making desorption the rate-limiting step. Late d-block transition metals such as zinc and cadmium have two valence electrons with a low hydrogen bond strength causing the rate-limiting step to be adsorption in contrast to their early d-block counterparts. Later noble metals such as silver and gold form fragile surface compounds and are chemically inert, due to the octet rule being satisfied, as they have no valence electrons to participate in reactions rendering both of them futile in catalytic hydrogenation. Between this, metals in Groups 8 to 10 have high catalytic activity, especially the platinum group metals costing

significantly more than most other metals. This is due to the high number of valence electrons, e.g., Palladium has 18 valence electrons making it highly reactive. It is necessary to decide on the most practical metal using a cost-benefit analysis. By observation, there is not much difference in the location of all the platinum group metals on the volcano plot implying marginal differences in hydrogenation catalyst capability. It is common knowledge that Ruthenium is a superior hydrogenation catalyst to Pd. However, its high cost does not justify its marginal improvement in activity over Pd.

2.3) Support materials

2.3.1) Metal oxides

Alumina

Alumina's reported minimum surface area is 0.1 to m^2/g with upper limit depending on the preparation method and calcination temperature, pore volumes between 0.1 and 1.5 cm^3/g, average pore sizes between 2 nm and 170 μm. It has an amphoteric nature making it versatile support compared to other types and has been used extensively to support Pd-based catalysts (Augustine, 1996). Numerous types of aluminas differ by crystalline structure and compositions depending on the degree of dehydration. Trihydroxides $Al(OH)_3$, Gibbsite and Bayerite, which upon loss of a water molecule lead to oxyhydroxides, AlO(OH), boehmite, pseudo **(φ)** boehmite and diaspore, further dehydration forms transition aluminas that have the generic formula $Al_2O_3.xH_2O$ with $0<x<1$. Complete dehydration gives corundum or γ-alumina (Augustine, 1996).

<u>Calcination temperature effect on reducibility, stability and TPR profile</u>

Hydrothermal treatment studies on Pd/alumina system indicate Pd crystallites completely oxidise at 600℃, but considerable dispersion occurs between 700℃ and 800℃. Smaller particles are easily oxidised and dispersed. Oxidation is necessary, but not a sufficient prerequisite for redispersion initiated at higher temperatures(Lieske and Voelter, 1985). Increasing calcination temperature causes shifts in peaks and their intensities of the TPR profile as at a lower calcination temperature of 600℃ almost all of the PdO is reduced at room temperature. With increasing calcination temperature this low-temperature peak diminishes as the high-temperature peak simultaneously increases in intensity and shifts to higher temperatures indicating an increase in more stable oxide and decrease in easily reducible oxide shown in figure 4 below(Lieske and Voelter, 1985).

Pd interaction with TiO_2

H_2 reduction over TiO_2-supported catalysts generates oxygen vacancies in coordinatively unsaturated cations near active metals, leading to changes in the catalytic activity and stability. Spillover of dissociatively chemisorbed hydrogen on noble metal promotes the reduction of TiO_2. TPR showed that Pd/TiO_2 where TiO_2 support calcined at 500℃ consumed the most hydrogen to reduce TiO_2. The TiO_2 reduction peak occurred at the lowest temperature (552℃) indicative of more vigorous promotion of the reduction of titania by the active Pd metal than other Pd/TiO2 titania support was calcined at higher temperatures(Kim *et al.*, 2013). During TPR due to strong metal-support interaction, SMSI, Pd particles were decorated by the TiO_2 overlayer, increasing the contact between Pd and TiO_2 enhancing the TiO_2 reduction rate elucidating that SMSI is strongest in that catalyst and the partially reduced TiO_2 support enriched the electrons of Pd.

Bimetallic Pd-Au and Pd-Ru supported on TiO_2

Bimetallic Pd-Au/TiO_2 was synthesised to hydrogenated Levulinic acid to $\gamma - valeroactone$. Monometallic Pd and Au catalyst were almost inactive yielding low conversions < 4 % after four hours, the bimetallic Pd-Au catalyst under identical conditions achieved 90 % conversion of LA at 97.5 % GVL selectivity (Luo *et al.*, 2015). An increase in LA hydrogenation activity was due to changes in surface reactivity of the bimetallic nano-alloys and thought to be the consequence of a combination of electronic and geometric effects elucidated below:

Electronic effects: Efficient mixing and electron transfer from Pd to Au in the Au-Pd catalyst suggested by collective characterisation results, namely the partial negative charge on Au observed from X-ray photoelectron spectroscopy XPS. Confirmation of an Au-Pd nano-alloy by STEM and EXAFS and evidence obtained by FT-IR for isolated Pd species and the proximity of Au and Pd. Significantly stronger CO adsorption on Pd than on Au-Pd alloy provides further evidence of Pd's substantial electronic modification upon nano-alloy formation with Au (Luo *et al.*, 2015).

Geometric effects: For Au-Pd systems, DFT (density functional theory) studies indicate incorporation of larger Au atoms in the Pd lattice (with has a smaller lattice constant than Au), results in a lattice mismatch causing tensile strain in the structure of these Au-Pd nano-alloys. This strain results in the metal sites ability to form bonds facilitating absorbance of species. Change in activity thought to be the result of a change in width and centre of d-band centres (for both Au and Pd) on alloying. In this case, a narrowing and upward shift of Pd's d-band due to the tensile strain results in enhanced chemical reactivity of these surface atoms (Luo *et al.*, 2015).

These positive results encouraged further work in alloying Pd and Ru supported on titania. Monometallic 1 wt. % Ru/TiO_2 gave a quantitative conversion after 40 min with 99 % selectivity to GVL which decreased to 93 % at longer reaction times of 2hr however Pd-Ru bimetallic catalyst molar selectivity remained stable at 99 % after 2hrs. There is not much room for improvement in the productivity of GVL from Ru/TiO_2 compared to Au/TiO_2 but alloying with Pd aids in sustaining GVL selectivity and improving catalyst stability (Luo *et al.*, 2015).

Unlike Au, little electron transfer between Ru and Pd is expected. Electronegativity of the two metals is the same; however, the inhibition of sintering of Ru is suggested to result from a stabilization effect. Pd on the surface dilutes and isolates the active Ru sites (Luo *et al.*, 2015).

Shoulder peaks appeared on the Ti 2p and O 1s XPS signals indicating electron transfer from Ru to TiO_2 with concomitant reduction of some of the Ti^{4+} into Ti^{3+}. The interaction between Ru and TiO_2 in the bimetallic Pd-Ru sample was weakened evidenced by longer Ru-O bond lengths. This was confirmed by EXAFS and the more limited

partial Ti reduction inferred from XPS resulting in sustained GVL selectivity as weakened interaction between support and metal effectively 'switches-off' any consecutive hydrogenation reactions halting production of undesired by-products (Luo *et al.*, 2015).

Pd/CeO_2 synthesized by one-pot redox method (Partially reducible support with oxygen vacancies)

A series of self-assembled Pd/CeO_2 catalysts with different Pd loadings ranging from 0.58 wt. % to 8.73 wt. % were synthesized via a facile one-pot redox method using $Ce(NO_3)_3{\cdot}6H_2O$, K_2PdCl_4 precursors and NaOH precipitant as under strong alkaline medium. The redox reaction between Ce^{3+} and Pd^{2+} facilitates the generation of nucleation centres, leading to the rapid in-situ formation of small-sized hybrids for Levulinic acid's hydrogenation (Y. Zhang *et al.*, 2017b). The Pd/CeO_2 hybrid was formed as per the following formula:

$Ce^{3+} + 3OH^- \rightarrow Ce(OH)_x^{\delta+}$ and $Ce(OH)_x^{\delta+} + PdCl_4^{2-} \rightarrow CeO_2$ + Pd + H_2O

No reduction or further treatment on Pd/CeO_2 hybrid performed and compared to conventional Pd/CeO_2 by precipitation and chemical reduction method. The hybrid's morphology was tuned by Pd loading as the morphology gradually shifted from square-shaped to sphere shape as the Pd loading increased from 0.58 wt. % to 8.73 wt. % which is an influential factor in catalytic performance. The Pd particle size decreases with an increase of Pd loading since the CeO_2 support is formed by the mutual redox reaction of Pd and Ce precursor, and can simultaneously encapsulate the PdNPs into its matrix preventing migration and agglomeration of Pd NPs into large particles (Y. Zhang *et al.*, 2017b).

XPS analysis performed to ascertain Pd's surface chemical state (5.82 %)/CeO_2 catalyst profiling two satellite peaks assigned to $3d_{5/2}$ and $3d_{3/2}$. Comparing Pd on activated charcoal where the peak shifts to a lower value support partial electron donation from cubic CeO_2 transferred to metallic Pd, leading to increased shielding of the nuclear charge and a weaker binding effect 3d electrons.

This mutual interaction of Pd-Ce is verified from the Ce XPS spectra. The ratio of $Ce^{3+}$to Ce^{4+} is induced and regulated by the presence of Pd (Pe-Ce mutual interaction) moreover the ratio of Ce^{3+} to Ce^{4+} is proportional to the amount of Pd. Oxygen vacancies will be generated with the alternation of cerium valence state to maintain change balance according to the below equation:

$[2Ce^{4+}, O2^-] \rightarrow [2Ce^{3+}, V_0] + \frac{1}{2}O_2$

Superior catalytic hydrogenation performance is attributed to Pd/CeO_2 catalyst with an increased electron density of Pd favourable for the dissociation of H_2 and the defects sites of CeO2 responsible for esterification of the intermediate into GVL (Y. Zhang *et al.*, 2017b).

Metal oxide supported Pd catalysed hydrogenation-amination

Pd supported on ZrO_2, Al_2O_3, and TiO_2 were synthesized and applied to the hydrogenation amination of Levulinic acid in which ZrO_2 was most active with no GVL by-product(Zhang *et al.*, 2016). ZrO_2, Al_2O_3, and TiO_2 supports are Lewis acidic oxides that may react with a carbonyl group via an acid-based interaction influencing reaction pathways. NMR and TPD were performed using probe molecules trimethyl phosphine (TMP) and acetone to understand the different support acidic properties. The prominent NMR peaks were assigned to the interaction of TMP with Lewis acid sites furthermore no peaks assigned to the interaction of Bronsted acidic protons could be identified confirming the presence and absence of Lewis and Bronsted acidic sites respectively in these oxides. The magic-angle-spinning NMR spectra of 2-C-acetone adsorbed on the supports confirm that ZrO_2 possesses more robust acidic sites than Al_2O_3, and TiO_2 evidenced by ZrO_2 intense peak at δ=224 ppm caused by the strong interaction of Lewis acidic sites with acetone. TPD profiles reassure this finding of acetone on the supports where in addition to low-temperature desorption peaks exhibited by all three supports, high-temperature peaks were exhibited by ZrO_2 and Al_2O_3 at 309℃, and 272℃ respectively. Te peaks mean that both supports strongly adsorb acetone by acid-base interaction with ZrO_2 as the superior ascorbate due to the higher desorption temperature. The IR spectra of acetone adsorbed on the supports resulted in and TiO_2 and Al_2O_3 exhibiting peaks at $\tilde{\nu}$=1724 and 1715 cm^{-1} assigned to the carbonyl bond of acetone. In the ZrO_2 spectrum, the vibration of the C=O bond appeared at $\tilde{\nu}$=1675 cm^{-1} corresponding to a redshift of 49 and 40 cm^{-1} from TiO2 and Al2O3, consistent with the more vital interaction of the primary carbonyl group with the Lewis acids ZrO_2 than other supports.

The strong Lewis acid-based interaction is deemed to significantly increase the carbonyl group's electrophilicity, promoting amination forming amine intermediates and preventing the hydrogenation of the C=O group to C-OH inhibiting GVL by-product.

Acidic sites for bifunctional catalysts

Bronsted and Lewis acid theory state that a Bronsted acid is a proton (hydrogen) donor to a Bronsted base while Lewis acid is a lone pair acceptor from a Lewis base, these definitions apply to complexes in solution as well as solid acids (Bnfoub and Pot, no date). A Lewis acid is typically an electron-deficient metal centre (electrophile) capable of coordinating electron-rich functional groups such as the oxygen atom from a carbonyl group and an alcohols hydroxyl group, thereby linking hydrogen donors and acceptor. Simultaneously, the adjacent base site attracts the hydrogen from the hydroxyl group weakening the O-H bond. Vital interaction between the Lewis acid site and hydroxyl oxygen induces more acidic hydroxyl hydrogen in the donor facilitating the base site's abstraction of

hydrogen. Conversely, elementary sites effectively abstract the hydroxyl hydrogen from the alcohol forming an alkoxide adsorbed on the adjacent Lewis acid site promoting hydride transfer (Gilkey and Xu, 2016)

The formation and function of Bronsted and Lewis acidic sites are different. Acidic hydroxyl groups exist on the surface of certain metal oxides as residual hydroxyl group after dehydration of metal hydroxide, or they are formed by the reaction of metal oxide with water hence the number of hydroxyl groups. In turn, Bronsted acidity depends mostly on the calcination temperature of the oxides. Standard surface Lewis acid sites are usually coordinatively unsaturated metal cations, in metal oxides or mixed metal oxides when surface hydroxyl groups are eliminated via elevated temperature calcination metal ions are exposed serving as Lewis acid sites(electron-deficient metal centres), common metal cations Al Sn and Ti serve as Lewis acid sites (Bnfoub and Pot, no date). Lewis acid sites catalyse MPV hydrogenation, explained under mechanisms in the application chapter while hydrolysis is catalysed by Bronsted acid sites hence it is imperative to balance the Bronstead and Lewis sites according to the catalytic process applicational objective function.

Carbon supports

Carbon nanotubes were treated with nitric acid before they were used as support material by Xu and co-workers to remove metal catalysts used to synthesise CNTs and incorporate oxygen-containing groups (Xu *et al.*, 2017). Incorporating Fe to produce a bimetallic Pd-Fe catalyst supported on CNT significantly increased the selectivity to hexitol from cellulose degradation. It is demonstrated that Fe incorporation could stabilize Pd^0 nanoparticles preventing reoxidation (Xu *et al.*, 2017). Since Fe is easily leached, it is suggested that support like TiO_2 be used instead to promote stability as it induces more vital interaction with Fe (Xu *et al.*, 2017).

Liu and co-workers have proven that incorporating rhenium to produce bimetallic Pd–ReO_x supported on activated carbon promotes direct /one-pot conversion of itaconic acid 2-methyl-1,4-butanediol (Liu *et al.*, 2016). TPR profiles exhibited a low-temperature peak for PdO reduction and high-temperature peak caused by reducing the functional group on the surface of activated carbon. Variations in reduction peaks of profiles of different ratios of metals ascribe to the interaction between ReO_x and activated carbon and synergy between Pd and ReO_x species. These impregnated catalysts displayed high surface area of over $1400\frac{m^2}{g}$ and a high degree of stability. Recycling tests entailed five repeated runs after which no significant changes in IA conversion and product distributions occurred. Structurally no noticeable differences were detected in XRD and TEM characterisation comparing fresh and used

catalyst (Liu *et al.*, 2016). No leaching of Pd was detected after ICP-AES analysis; only an insignificant amount of Re was detected in the reaction solution. Pd–ReO_x/C catalysts showed superior recyclability than Pd–FeO_x/C were reported in succinic acid hydrogenation (Liu *et al.*, 2016).

Nitrogen-functionalized ordered mesoporous carbons were readily obtained by post-synthesis with nitrogen loading as high as 8.6 wt. % and well preserved mesoporous structure by incorporation of nitrogen-hybrids into FDU-type ordered mesoporous carbon (OMC) materials with NH_3 and melamine as a nitrogen source, yielding N-incorporated OMC (NOMC)(Li *et al.*, 2013). NH_3 was reported as the superior nitrogen source as the resulting hybrid material displayed a significant increase in surface area and pore volume. These N-doped carbons are supports immobilizing Pd nanoparticles. N-doping could also change the support's physicochemical and electronic properties and serve as basic or coordination sites to stabilize the small metal NPs or activate some unique substrate (such as phenol in its hydrogenation) (Li *et al.*, 2013).

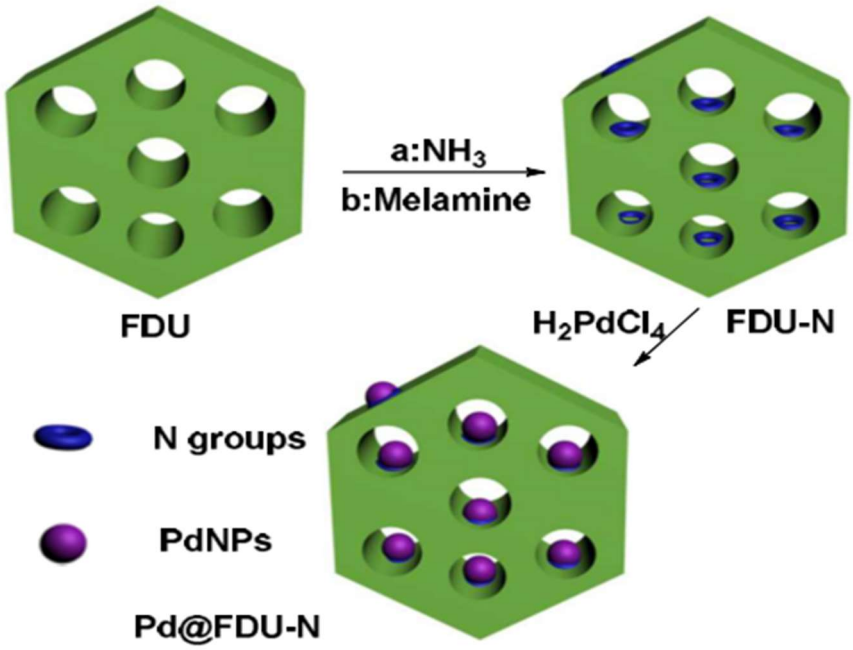

Figure 2.2:Illustration of the route to synthesize Pd nanoparticles supported on NOMCs(Li et al., 2013)

The stability and catalytic activity increase in phenol hydrogenation are due to the synergy of two interactions:

1) N-doping on carbons' surface stabilizes the Pd (PdNPs) nanoparticles during the liquid phase reaction through electron donation from nitrogen to the metallic PdNPs.

2) Phenol substrate would interact with the N-incorporated groups on the surface of the mesoporous carbon support through the hydroxyl group-nitrogen interaction enabling more effective adsorption of the phenol than the pure carbon.

The stabilizing role of the N-doped functionalities is determined by omitting nitrogen dopant and impregnating the mesoporous carbon with Pd mostly distributed on the external surface of the OMC but not inside the channels confirmed by STEM and TEM imaging. Comparison of particle size distribution with N-doped analogues reveals that Pd particle size is smaller on NOMC support due to the confinement effect where the size of PdNPs formed on the supports external surface is slightly larger than those formed and stabilized in the mesochannels restricting the growth of the PdNPs (Li *et al.*, 2013).

The advantage CNT support boasts due to the absence of micropores and the Pd being readily accessible on the surface of CNT is that pore diffusion mass transfer limitations are eliminated which is not possible in supports containing micropores such as Pd/SiO_2 and Pd/Al_2O_3 support. The reaction pathway is temperature-dependent as at higher temperatures the adsorptive capabilities of benzyl alcohol intermediate on the support is decreased at higher temperatures over Pd/CNT halting further hydrogenation to toluene on the CNT support.

2.4) Mechanisms

2.4.1) Motivation for transfer hydrogenation

The low solubility of molecular hydrogen in most solvents necessitates high hydrogen pressure to achieve the desired conversion. Liquid phase organic hydrogen donors are advantageous in comparison to high-pressure, flammable hydrogen gas, due to enhanced solubility of the hydrogen donor in the liquid phase eliminating the safety hazard and economic barrier of implementing high-pressure infrastructure associated with high-pressure hydrogen gas (Gilkey and Xu, 2016). For an alcohol, the spent hydrogen donor is either an aldehyde or ketone can be separated for constructive use example in carbon chain growth reactions through aldol condensation (Gilkey and Xu, 2016). The degree of freedom of the catalyst design is increased by using catalytic transfer hydrogenation (CTH) because donors could transfer hydrogen via different mechanistic pathways, for example, intermolecular hydride transfer can be used to control selectivity.

2.4.2) Mechanisms types

Homogenous CTH mechanisms infer Heterogeneous CTH mechanisms by comparison. Transfer hydrogen occurs via direct transfer or the metal hydride route. Deuterium (D) is one of two stable isotopes of hydrogen. Deuterated hydrogen donors differentiate the underlying reaction pathways as D's isotopic purity can be detected in products tracking different hydrogen atoms' movement throughout the mechanism (Gilkey and Xu, 2016).

2.4.2.1) Direct transfer route (MPV)

The Meerwein−Ponndorf−Verley (MPV) mechanism is when an alcohol is the hydrogen donor to reduce a carbonyl group via the direct transfer pathway the α-hydrogen transfers from the α-carbon of the alcohol, in a concerted step via a six-membered-ring intermediate without metal hydride formation. A base in any form whether, ligand, solvent molecule or dissolved basic species enhances reactivity in homogenous CTH by extracting the hydroxyl proton to be transferred to the carbonyl group corresponding with the heterogeneous direct CTH pathway where solid catalyst exhibiting electron-deficient Lewis acid sites and neighbouring base sites drive CTH reactions via MPV mechanism (Gilkey and Xu, 2016).

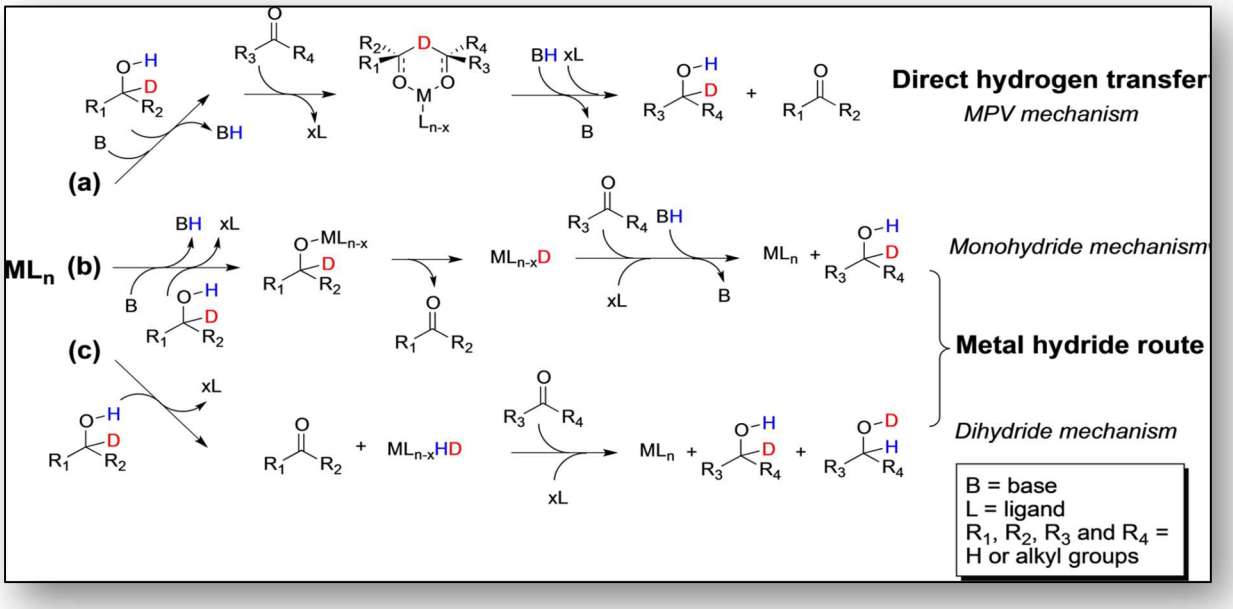

Figure 2.3: Homogenous transfer hydrogenation mechanisms (Gilkey and Xu, 2016)

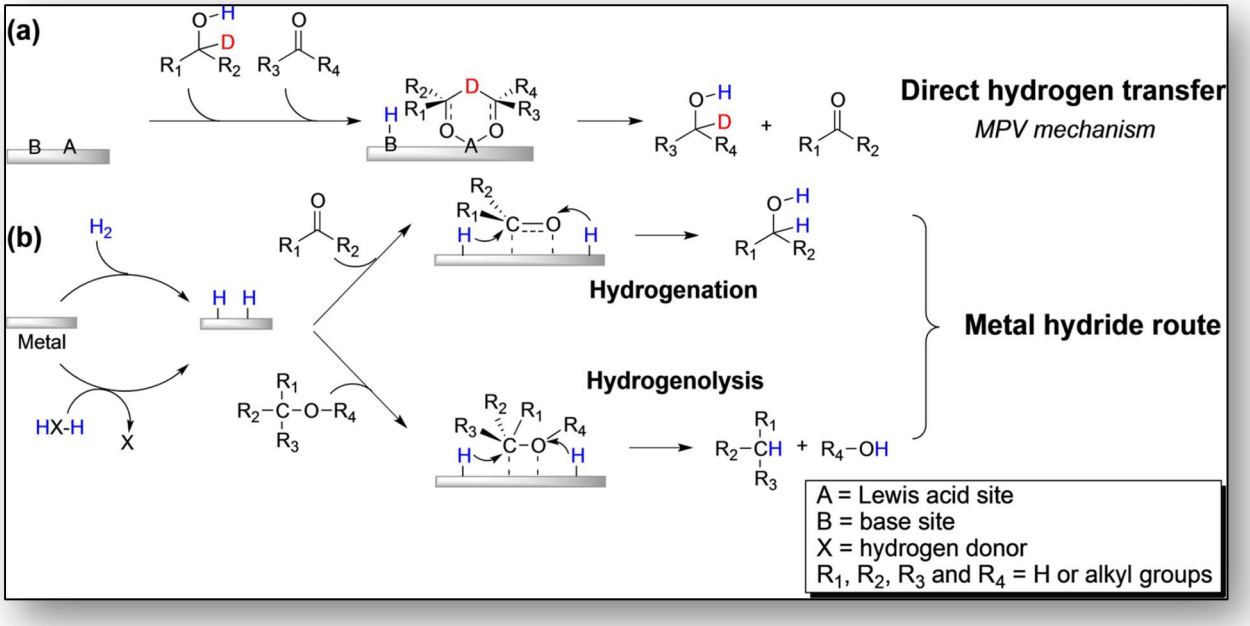

Figure 2.4: Heterogeneous transfer hydrogenation mechanism (Gilkey and Xu, 2016)

2.4.3.2) Acid-base pair sites facilitating direct transfer route

Acid base-pair sites can facilitate CTH between an alcohol and carbonyl group via the direct hydrogen transfer mechanism as hydride formation on acid-base sites is difficult. Both Lewis acidic and basic sites are essential to mediate CTH following MVP mechanism. The role of a Lewis acid site, typically an electron-deficient metal centre, is to bond with the electron-rich oxygen in the hydroxyl group and carbonyl group, linking both hydrogen donor and acceptor while adjacent base site attracts the hydrogen from the hydroxyl group weakening the O-H bond. Stronger interaction between the Lewis acid site and hydroxyl oxygen induces more acidic hydroxyl hydrogen in the donor facilitating the base site's abstraction of hydrogen. Conversely, strongly basic sites effectively abstract the hydroxyl hydrogen from the alcohol forming an alkoxide adsorbed on the adjacent Lewis acid site promoting hydride transfer (Gilkey and Xu, 2016). The preceding two statements indicate that both strong acids and strong bases facilitate CTH, but the coexistence of strong acid and basic sites on the same catalysts is unlikely as either acid or base property of a catalyst could dominate an acid-base pair needed to complete the catalytic cycle.

2.4.3.3) Metal hydride route using a hydrogen donor

Subcategories of the metal hydride route are the monohydride and dihydride route. The monohydride route is characterised by hydride formation between hydrogen from the α-carbon and the metal distinguished from the dihydride route where both the hydrogen from the hydroxyl group and α-carbon are transferred to form metal hydrides. These hydrogen atoms from two different sites were chemically equivalent using isopropyl alcohol as a hydrogen donor and deuterating the α-carbon and not the hydroxyl group; both hydrogens were equally likely to bond the carbon or oxygen from the carbonyl group. Assumption of Chemical equivalence of all adsorbed hydrogen atoms leads to the hypothesis that mechanisms and product distributions using hydrogen gas or an organic hydrogen donor should, in principle be equivalent (Gilkey and Xu, 2016).

2.4.4) Pd dynamic redox cycle during hydrogenation reaction

Heterogeneous catalytic mechanisms differ from homogeneous mechanisms in that they rely on the surface chemistry of the active metal sites existing in clusters, either crystallites or single atom sites. Mechanisms are developed by analysing homogenous counterpart mechanisms. The figure below illustrates Pd's plausible catalytic redox cycle during the hydrogenation of an alkene to alkane tracking oxidation state as Pd traverses through cycle regenerating to initial oxidation state to begin the next cycle. Turnover frequencies are calculated from selectivity

and yield rate data, which is an indirect way to measure how many cycles per second the catalyst, traverses because the catalytic cycle and reactants to products conversion are conjugate processes as per figure below.

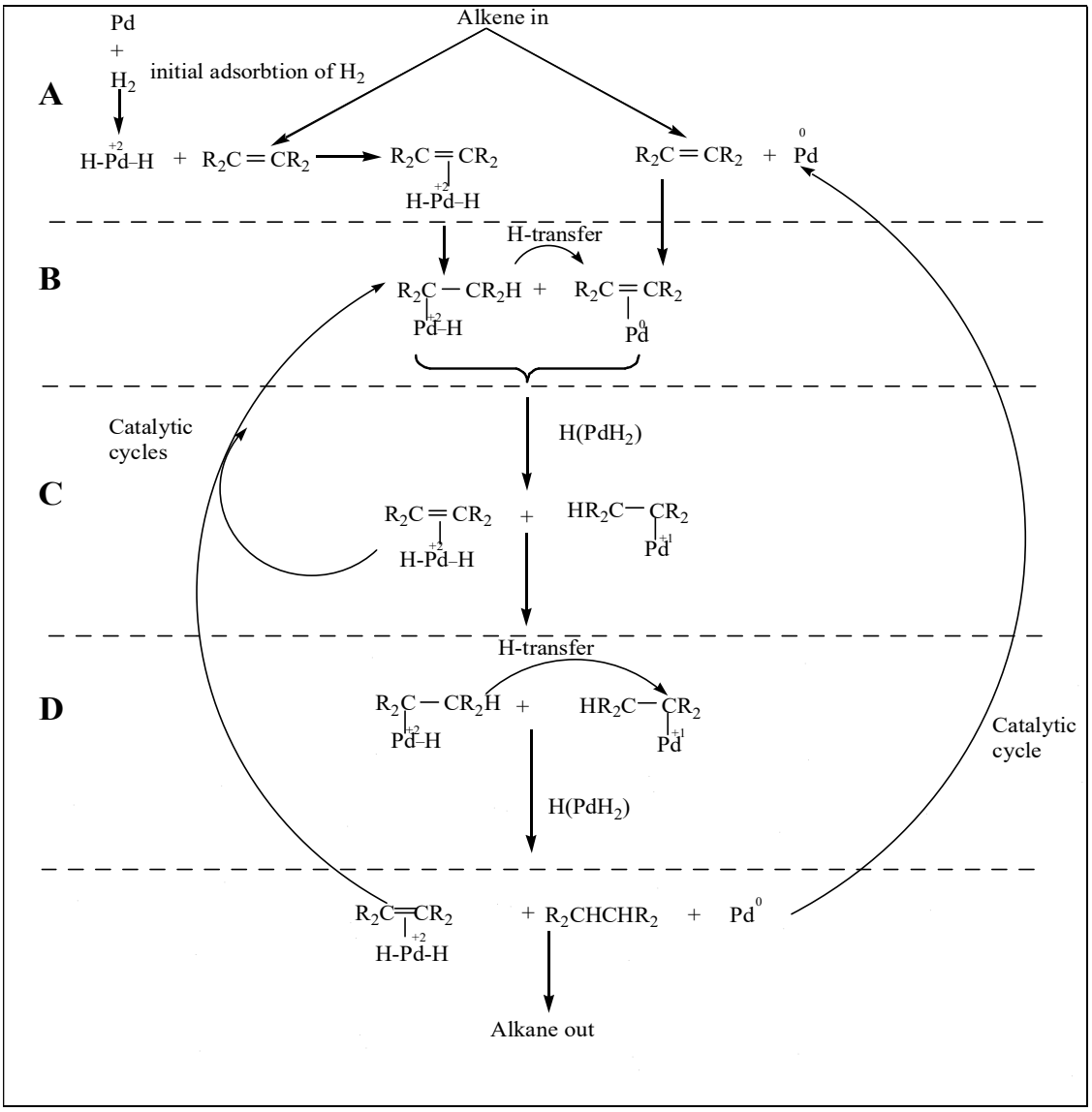

Figure 2.5:Pd catalytic cycle adapted from (Entwistle, 1985)

Salient mechanism features

Seeing that some reactions occur in parallel, the mechanism is segmented into successive rows simplifying interpretation.

Row A: Hydrogen is adsorbed onto Pd^0 increasing the oxidation state to Pd^{+2}, the alkene substrate then approaches to adsorb onto Pd, parallel to this the alkene attaches to Pd^0.

Row B: Alkene substrate bonds to $Pd^{+2}$and hydrogen bonds to the adjacent carbon, reducing the double bond to a single bond.

Row C: In one concerted effort an unstable intermediate is formed (Pd^{+1}) by the alkene binding to Pd^{0} and hydrogen transfer from a neighbouring adsorbed alkane from row B. Parallel this the other intermediate in this step is recycled to the previous step contributing to the recycle loop.

Row D: The recycled intermediate from C is also carried forward and transfers hydrogen to the unstable intermediate which detaches from Pd^{+1} forming the alkane product reducing Pd^{+1} back to Pd^{0}.

CHAPTER THREE: MATERIALS AND METHODS

Table 3.1 List of materials

List of materials	
Material	**Use/description**
Aluminium nitrate nonahydrate	Precursor salt
Tin pentachloride	Precursor salt
Polyvinylpyrrolidone (PVP)	Templating agent
Palladium chloride	Active metal solution
Ethanol	Solvent
Sodium borohydride	Reducing material for palladium
Ethylene glycol	Solvent
Nitric acid	Dissolvent for palladium

Literature review findings reveal that amphoteric mixed metal oxide alumina-tin-based support material exhibits Lewis and Bronsted acidic sites facilitating transfer hydrogenation via the Meerwein-Ponndorf-Verley mechanisms direct transfer route. The initial methodology entailed screening the synthesis method by restricting the reactants to 2 g resulting in a small amount of support material. After meeting characterization specifications, the final methodology entailed synthesizing and characterizing 5 g of product. This final product was impregnated with Palladium nanoparticles before calcination and characterizing. A flow chart below illustrates the logic behind the experimental design.

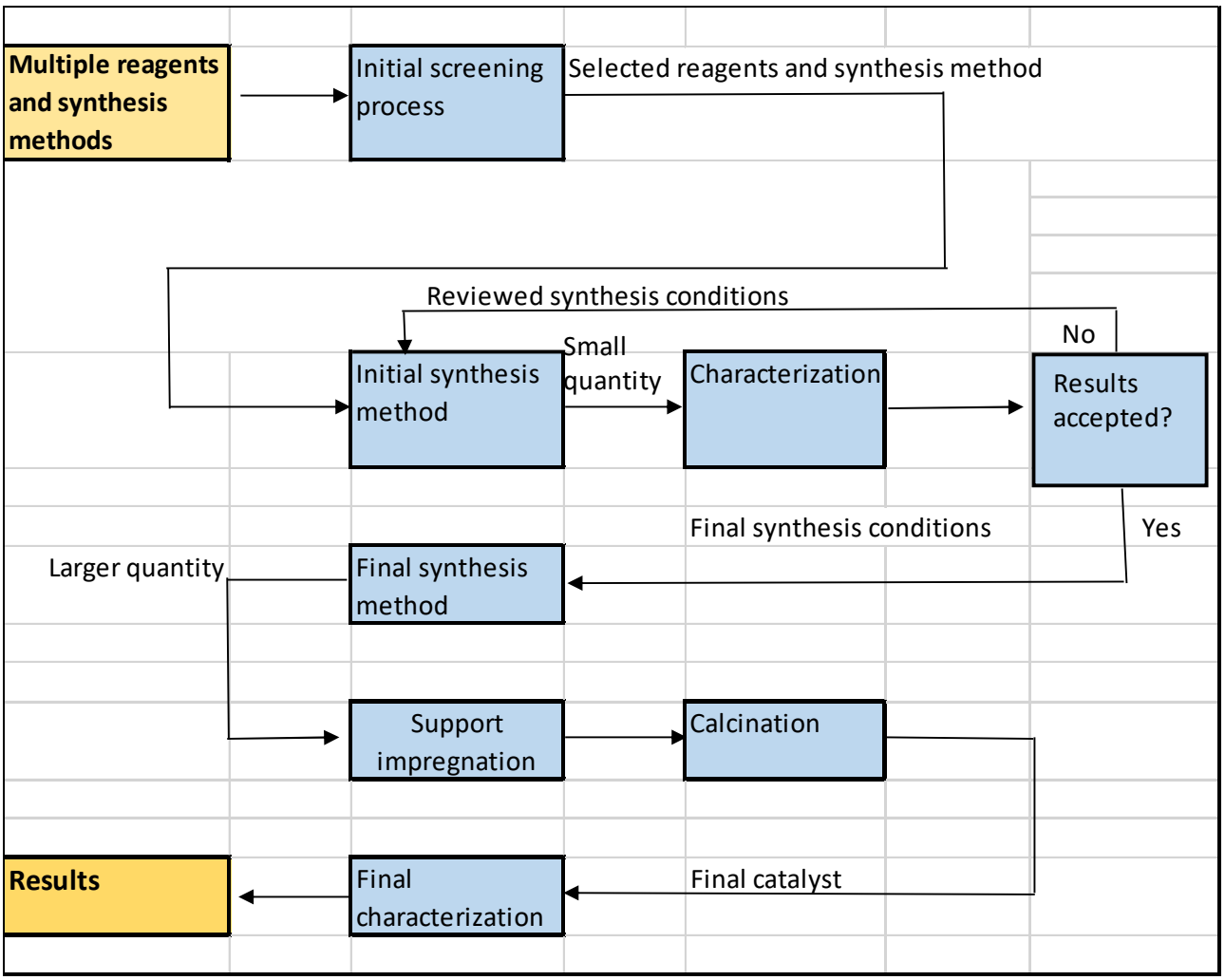

Figure 3.1: Experimental design flow chart

3.1) Initial methodology

An equivolume mixture of ethanol and water was prepared as the solvent. Add 1 g of Polyvinylpyrrolidone (PVP), a templating agent used to direct nanoparticle growth in its pores to solvent while heating on a hot plate at 70℃ and magnetic stirrer set at 500 rpm until all PVP dissolves. Sonicate solution if need be until all PVP dissolves. Add 2g of precursor salts, Aluminium nitrate nonahydrate and Tin pentachloride to solvent (2g split shown in sample calculations below). Reflux solution using reflux condenser at 100℃ for 1 minute dissolving precursor salts. Reflux solution for two hours (inside reaction temperature measured as (80℃ with thermometer). Transferred solution into microwave vessels and inserted into microwave digester with the method set at 100 % stirring speed, 1000 W,

180℃, 22 bar nitrogen, and 2 hr. Centrifuged the solution at 4000 rpm for 10 minutes thereafter discard the supernatant fluid from centrifuge tubes washing the sediment with ethanol. Repeat washing twice to remove chloride impurities. Added ethanol to sediment to remove non-polar impurities and centrifuge. Transfer wet solids into heat resistant glass tubes and dry in the oven for 24 hr at 100℃. Weigh samples before calcining at 500℃ at a ramp rate of $1℃/min$ held at 500 ℃ for 3 hours. Degas samples for 2 hours at 150 ℃ to remove moisture. Characterise the synthesised metal oxide support materials.

3.2) Support impregnation

The deposition was achieved by creating a solution of suspended Pd nanoparticles from its precursor salt $PdCl_2$ that was added to 1g of support material driving the impregnation process by capillary action inside the support pores material.

Preparation of Pd precursor solution.

Prepare 150 ml of impregnation solution solvent as an equivolume mixture of ethylene glycol and ethanol (75ml each per vessel for five vessels. The calculated amount of $PdCl_2$ precursor salt (0.319 g) was added to the solvent from the previous step. After 3 hours of sonication add 6 ml of nitric acid to completely dissolve $PdCl_2$. Heat the solution on a hotplate and stirred at 400 rpm for 5 min increasing precursor salt dissolving rate. Prepare a solution of 12 g PVP in 100 ml ethanol and distribute equally amongst the five vessels. Prepare sodium borohydride as a reducing agent by mixing 6 g of sodium borohydride pellets in 50 ml of water and swirling until all the sodium borohydride dissolved. At a reflux temperature of 100 ℃ add 10 ml of the sodium borohydride solution prepared in the previous step dropwise to the solution in each of the five vessels, changing its colour from milky reddish to brown reducing the Pd^{2+} to Pd^0 oxidation state forming Pd nanoparticles.

Support impregnation with Pd

Increase the reflux temperature to 200℃ before adding 1 g of support material to palladium nanoparticle solution. Reflux the solution for 30 min at 200℃ before decreasing temperature to 100℃ refluxing for 15.5 hours. Wash samples with water and ethanol, leaving particles to settle, if necessary, by removing the supernatant fluid with a dripper minimising perturbation of nanoparticles in suspension above the sediment. Pd nanoparticles are now deposited onto the support material, but the Pd and support material's interaction is weak as no bonding, chemisorption or physisorption occurred. Although Pd^0 is required for hydrogenation reaction, samples were calcined at 500℃ at a ramp rate of 3 ℃/min chemically binging Pd to the support as PdO by infusing Palladium into

the lattice structure of the support material leaving Pd in +2 oxidation state ending the synthesis omitting activation by reduction by hydrogen.

3.3) Sample calculations

For 40 mole % Support

A) Number of moles of Al in Aluminium Nitrate nonahydrate precursor salt, nAl =1 mole Al per 1 mole Al salt.

B) Number of moles of Sn in Tin pentachloride precursor salt, nSn =1 mole Sn per 1 mole Sn salt.

C) 40 % Sn in the final catalyst support implies $(moles\ Sn)/((moles\ Sn + moles\ Al)\ ) = 0.4$

Using equations A and B to rewrite equation C, we get:

$$\frac{moles\ Sn\ salt}{(moles\ Sn\ salt\ + moles\ Al\ salt)} = 0.4$$

$Number\ of\ moles = \frac{Mass}{Molar\ mass}$, substitution into the above equation results in the expression below.

$(Mass\ Sn\ salt \times Molar\ mass\ Sn\ salt)/\{moles\ Sn\ salt \times Molar\ mass\ Sn\ Salt\ + moles\ Al\ salt \times Molar\ mass\ Al\ salt\} = (350.6 Sn\ salt\ mass)/(350.6 Sn\ salt\ mass + 375.13 Al\ salt\ mass) = 0{,}4$…equation 1

2 g total precursor salts constraint implies that the Mass of Sn salt + Mass of Al salt=2 g…. equation 2

The system now has zero degrees of freedom with two unknowns and two equations.

Solving 1 and 2 simultaneously yields 0,7633 g Sn salt and 1,2328 g Al salt.

Solvent = 25 ml ethanol + 25 ml water= 50 ml solvent.

5 ml nitric acid used as a precipitant.

Theoretical mass that should ideally be formed assuming all aluminium goes to Al_2O_3 and all tin goes to SnO_2 after calcination =0.495 g

Actual mass obtained=0.333 g therefore % yield = ideal mass yield / actual mass yield =67.27 %

The amount to be synthesised in the final methodology was 5 g of the final product. Therefore, the scaling factored used was target mass/experimental yield=5 g/0.333= 15.015 g and a 20 % safety factor was employed yielding a new scaling factor of 18.018.

To work around the challenge of limited ethanol availability, the solvent basis before scaling up was assumed to be 30 ml per batch instead of 50 ml.

CHAPTER 4: RESULTS AND DISCUSSIONS

Physisorbtion

The surface area of 90% Alumina support was 261,43 m^2/g after calcination, which is extremely high and desirable for these materials. The surface area would be higher if the support were pure alumina as the including tin in the composite microstructure decreases the surface area to 72.22 m^2/g at 50% tin as can be inferred from the trends in table 4.1 and figure 4.1 below. The undesirable surface area does not imply that the catalyst with less tin is superior as tin was introduced for its acidity modifying properties to support interaction with the substrate molecules. This feature can be checked with in-situ FTIR and TPD characterisation tests. The entire composite support surface area decreases marginally after impregnation with Pd for all samples as expected due to reduced pore volume, figure 24.

Table 4.1: Physisorbtion results before and after impregnation of final catalyst

Physisorbtion results	**BET surface area comparison(m^2/g)**		**Pore size width comparison (nm)**		**Pore Volume comparison *cm3/g**	
Sn molar composition	Before impregnation	After impregnation	before impregnation	After impregnation	before impregnation	After impregnation
10	261,43	233,43	9,53	9,82	0,624	0,573
20	204,49	172,36	9,02	9,77	0,4613	0,421
30	149,01	122,65	8,09	8,775	0,303	0,269
40	120,67	94,95	7,42	8,28	0,224	0,196
50	72,22	54,95	6,87	7,895	0,124	0,122

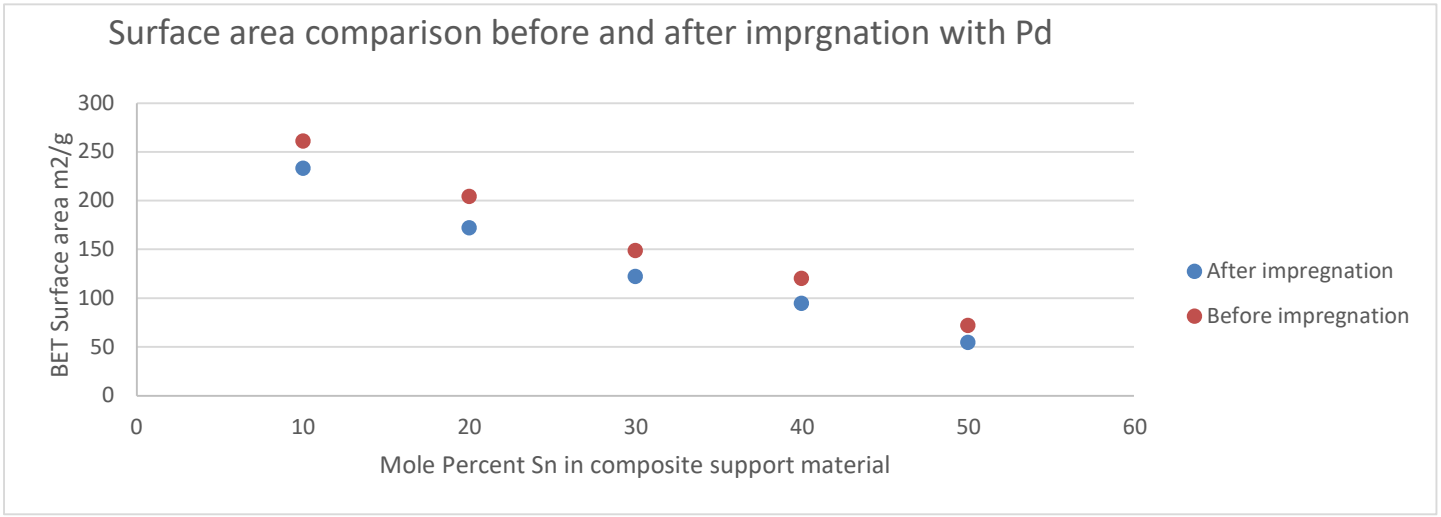

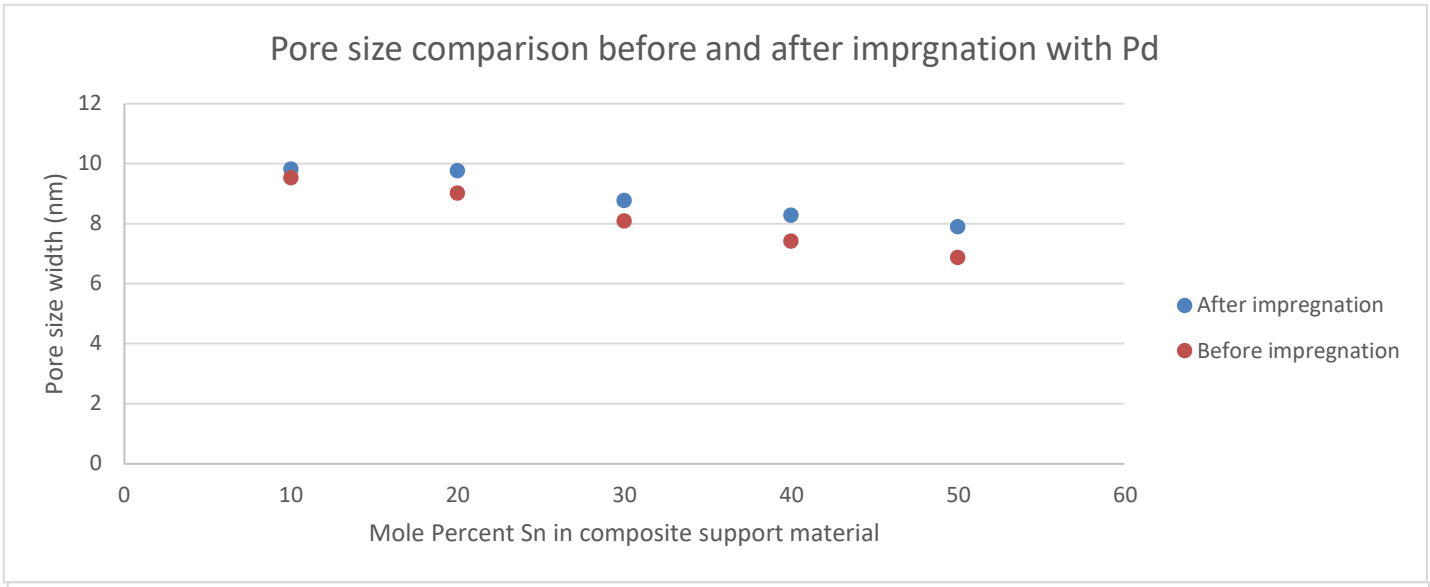

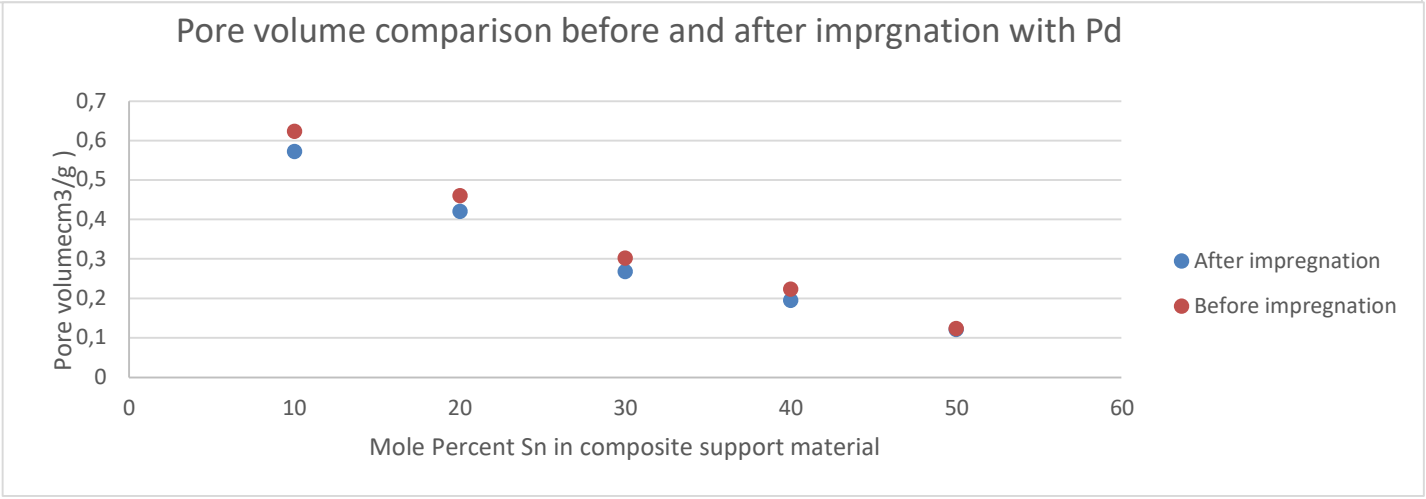

Figure 4.1: Physisorbtion results

EDX analysis

It was possible to perform nitrogen physisorbtion and XRD analysis on all samples, however, due to limited resources, only two slots were available for SEM imaging and EDX mapping hence analysis was performed on the first and last samples yielding the endpoints of the sample space.

EDX

EDX spectra confirm tin, aluminium and Palladium in their elemental form showing that the quantities are close to the nominal amounts. Maps indicate high density in tin even in the 10 % Sn support as tin is a denser element than Al. Deconvoluted EDX maps display the dispersion, evenly dispersed PdNPs are desired over clumped nanoparticles, and one anomaly site displayed a clump, figure 4.4 with the others being evenly dispersed. EDX analysis was performed per site, and the Pd percentage varies above and below the expected Pd loading but on average will give the expected loading.

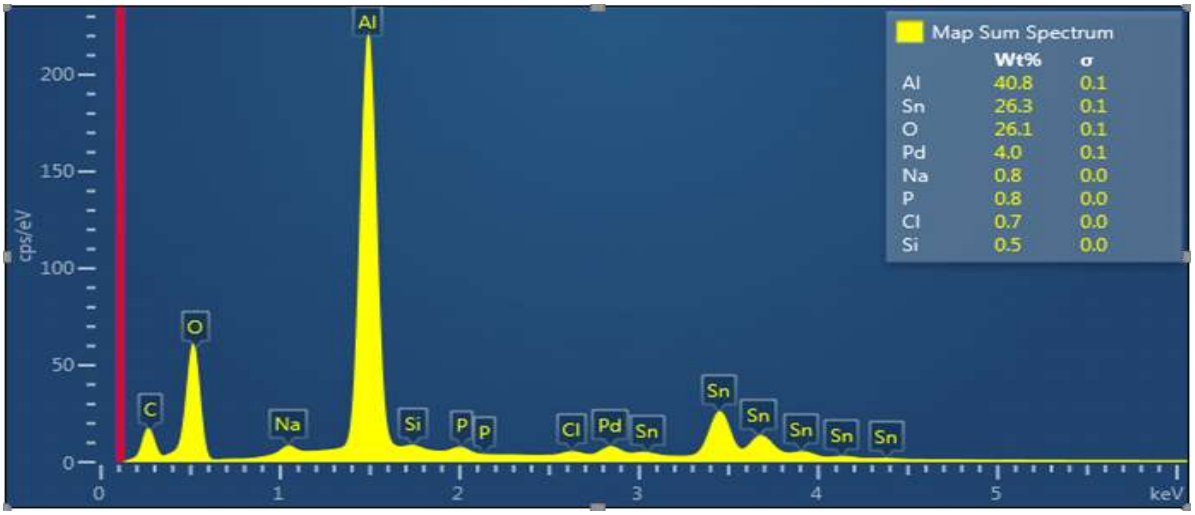

Figure 4.2: Site 1 10 mole% Sn catalyst elemental analysis map spectrum

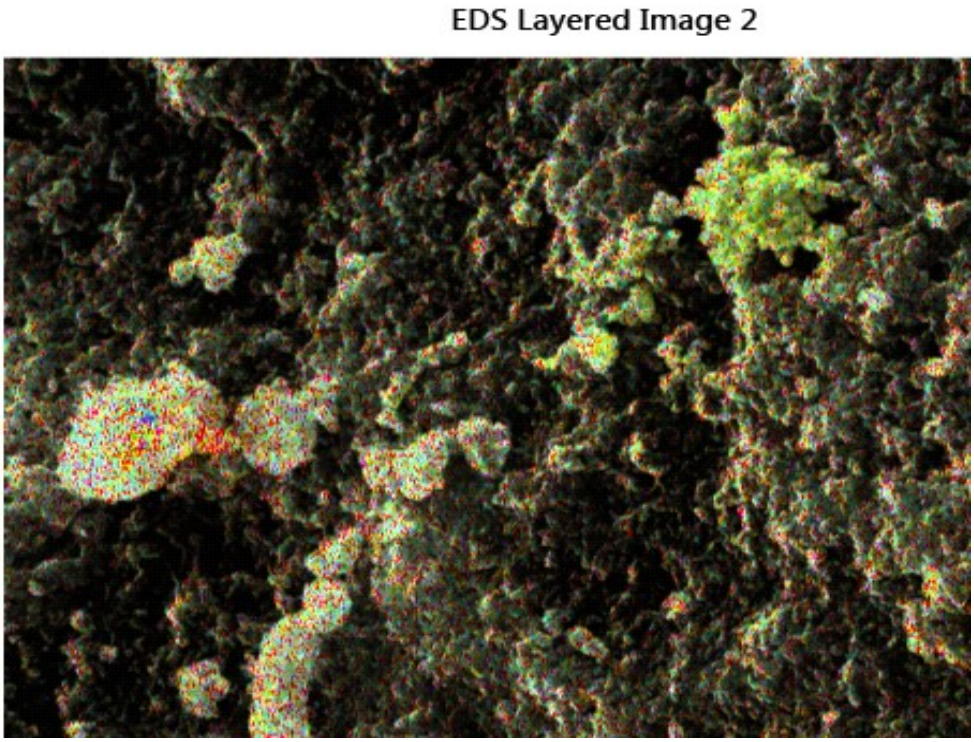

Figure 4.3: Layered 10% Sn site one map

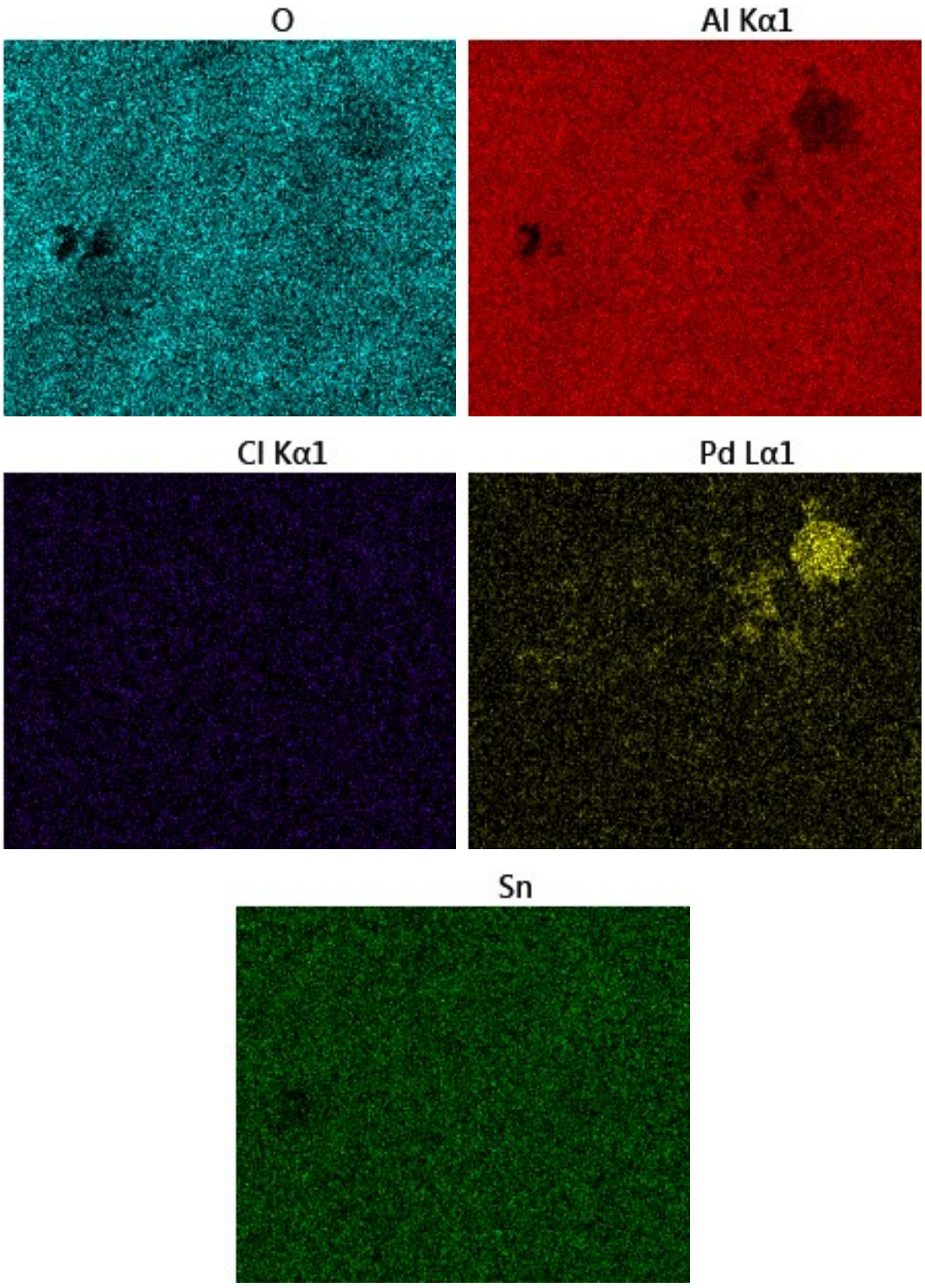

Figure 4.4: Deconvoluted 10 mole % Sn site one map

EDX site2 for 10% Sn

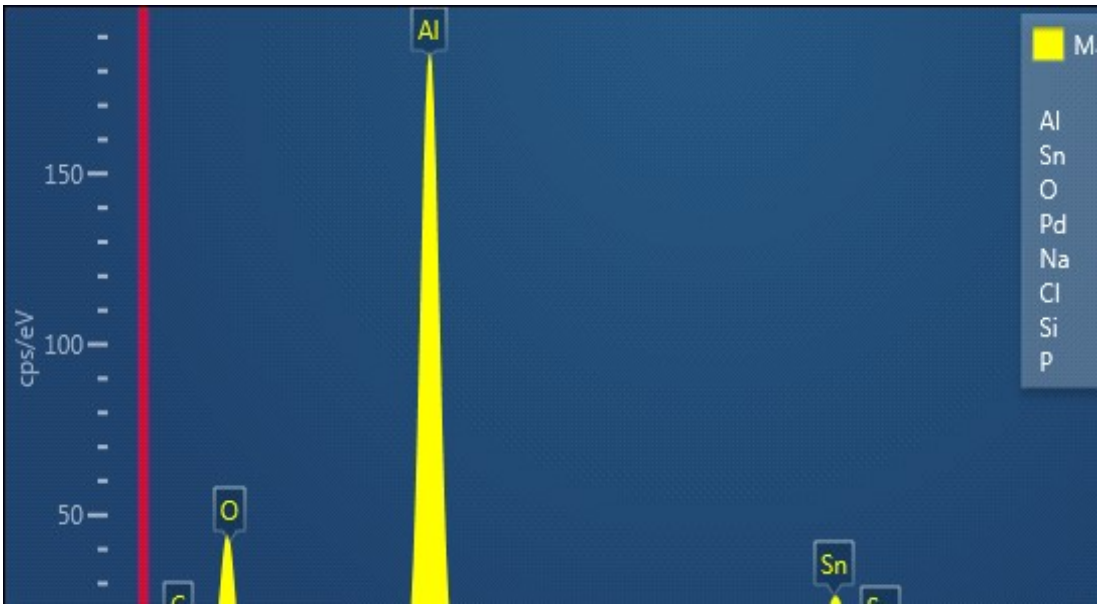

Figure 4.5: Site 2 10 mole % Sn catalyst elemental analysis map spectrum

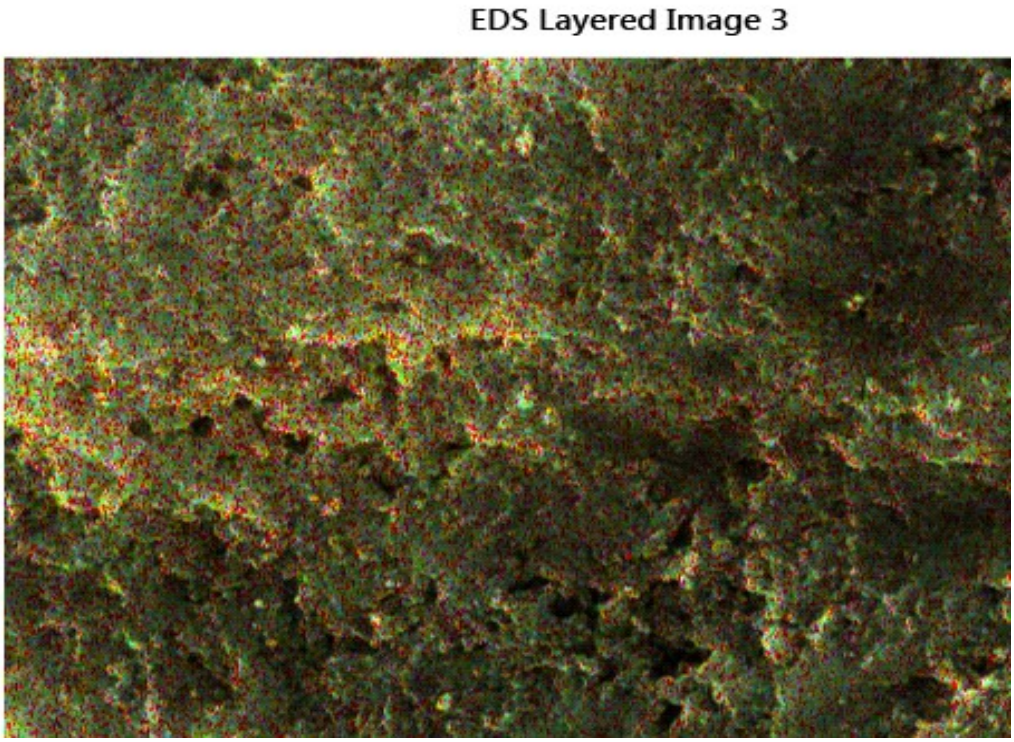

Figure 4.6: Layered 10% Sn site two map

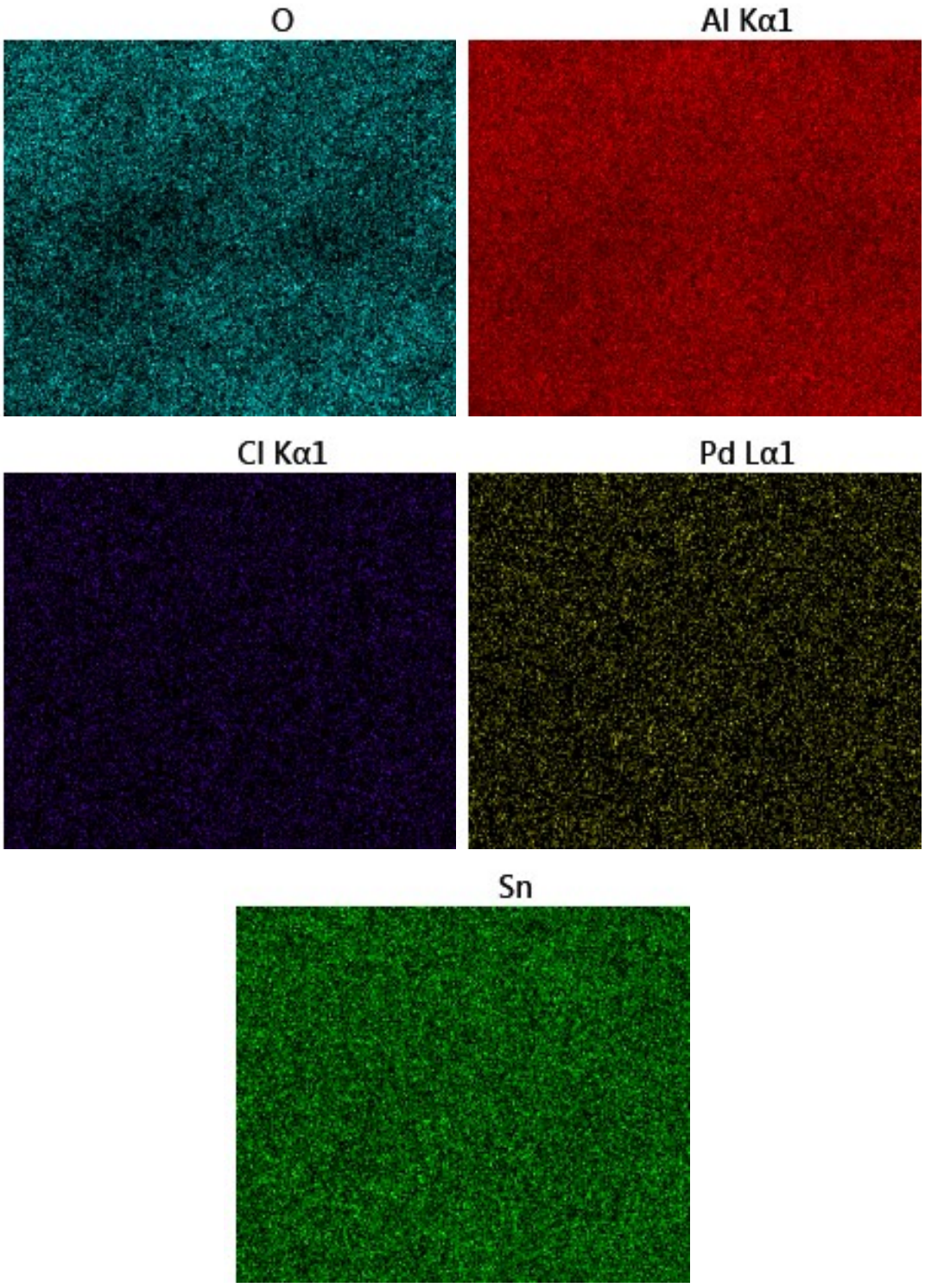

Figure 4.7: Deconvoluted 10 mole % Sn site 2 maps

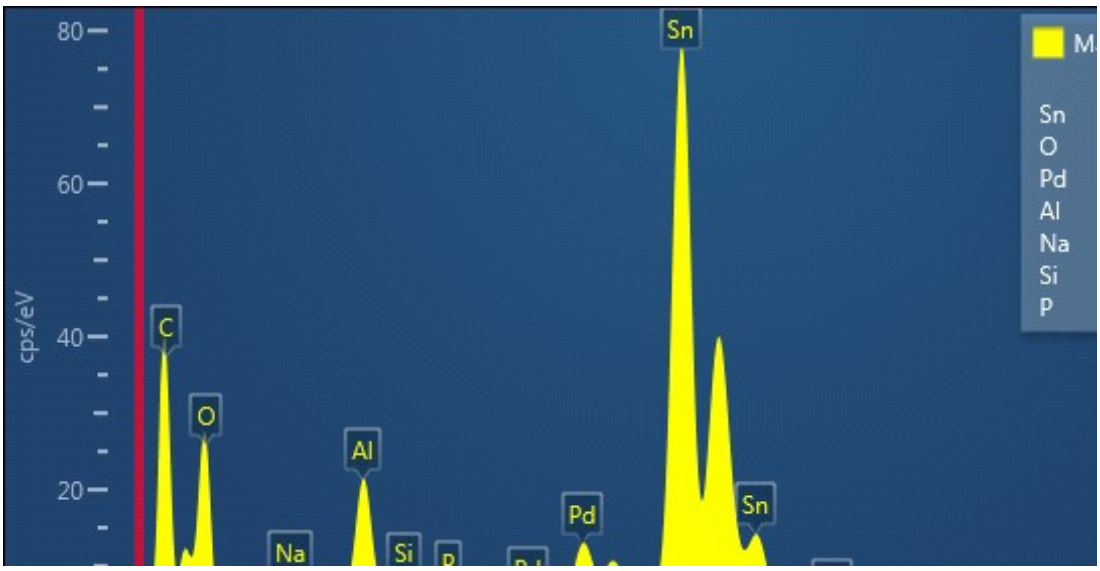

Figure 4.8: Site 1 50 mole % Sn catalyst elemental analysis map spectrum

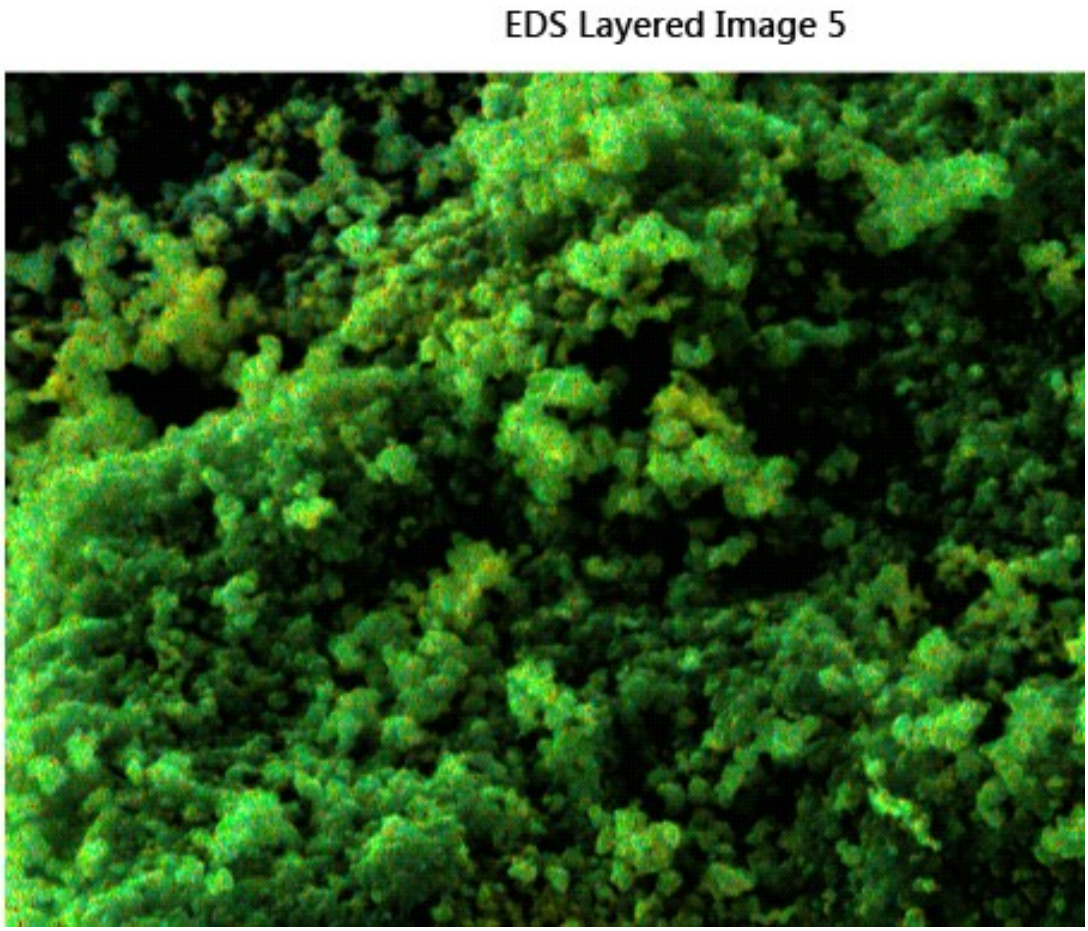

Figure 4.9: Layered 50 % Sn site one map

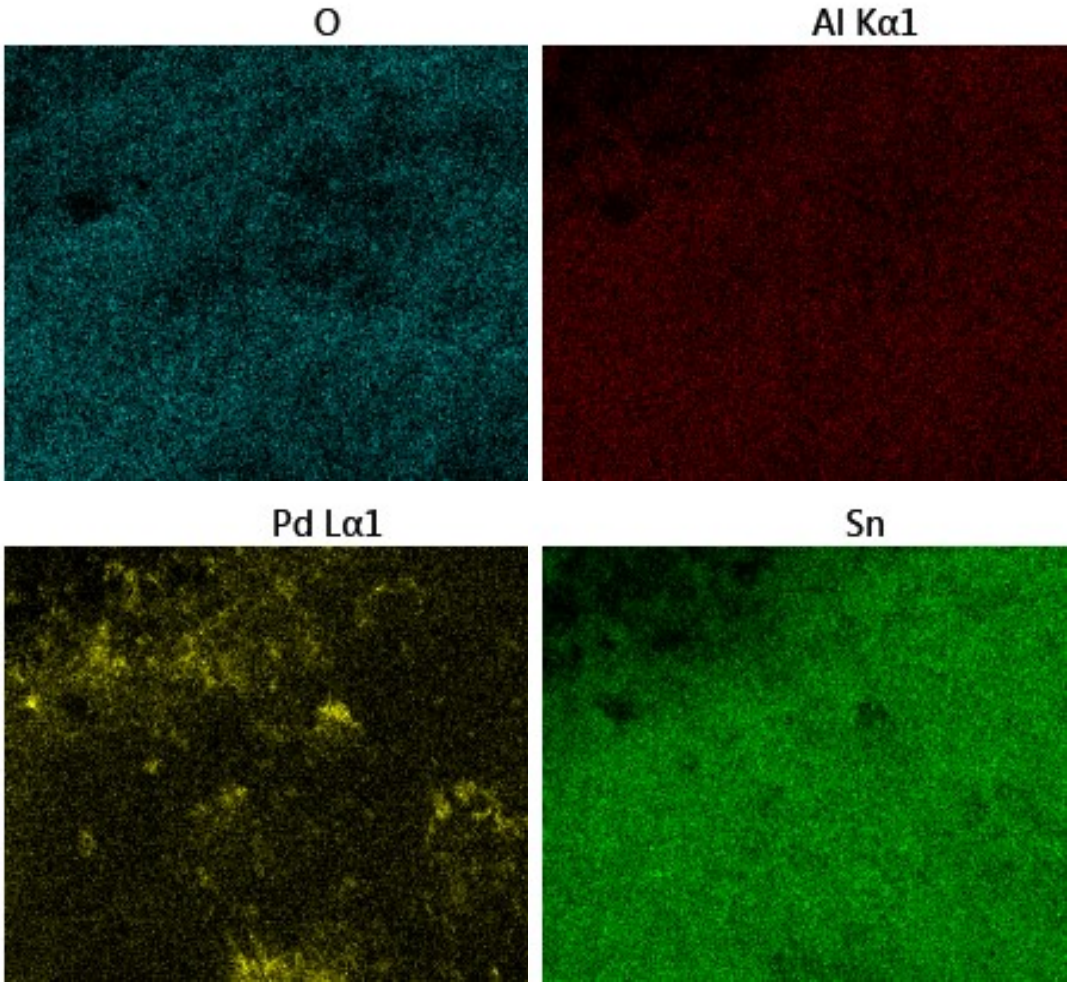

Figure 4.10: Deconvoluted 50 mole % Sn site one maps

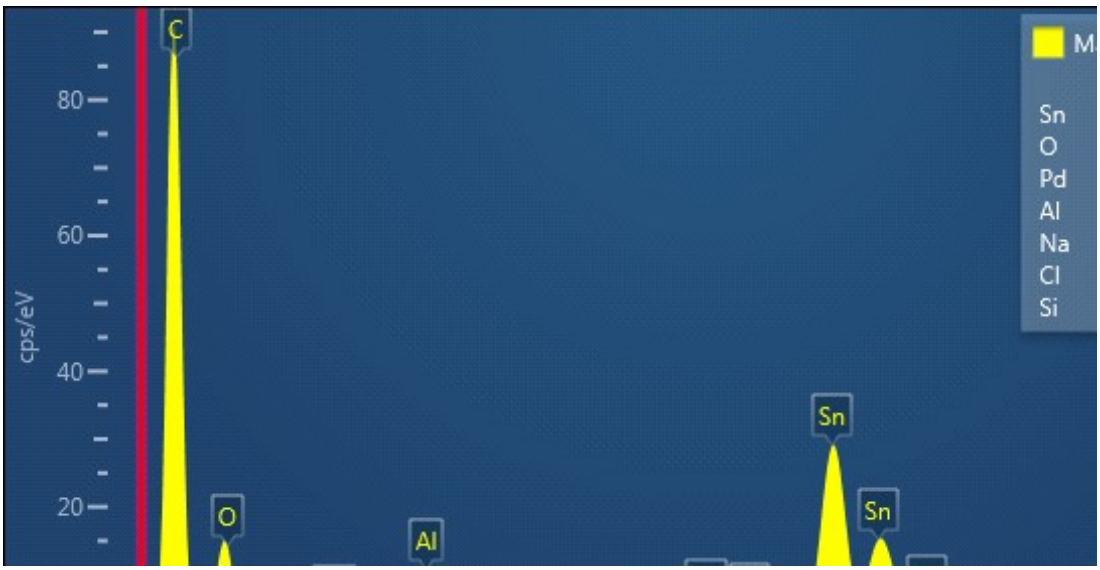

Figure 4.11: Site 2, 50 mole % Sn catalyst elemental analysis map spectrum

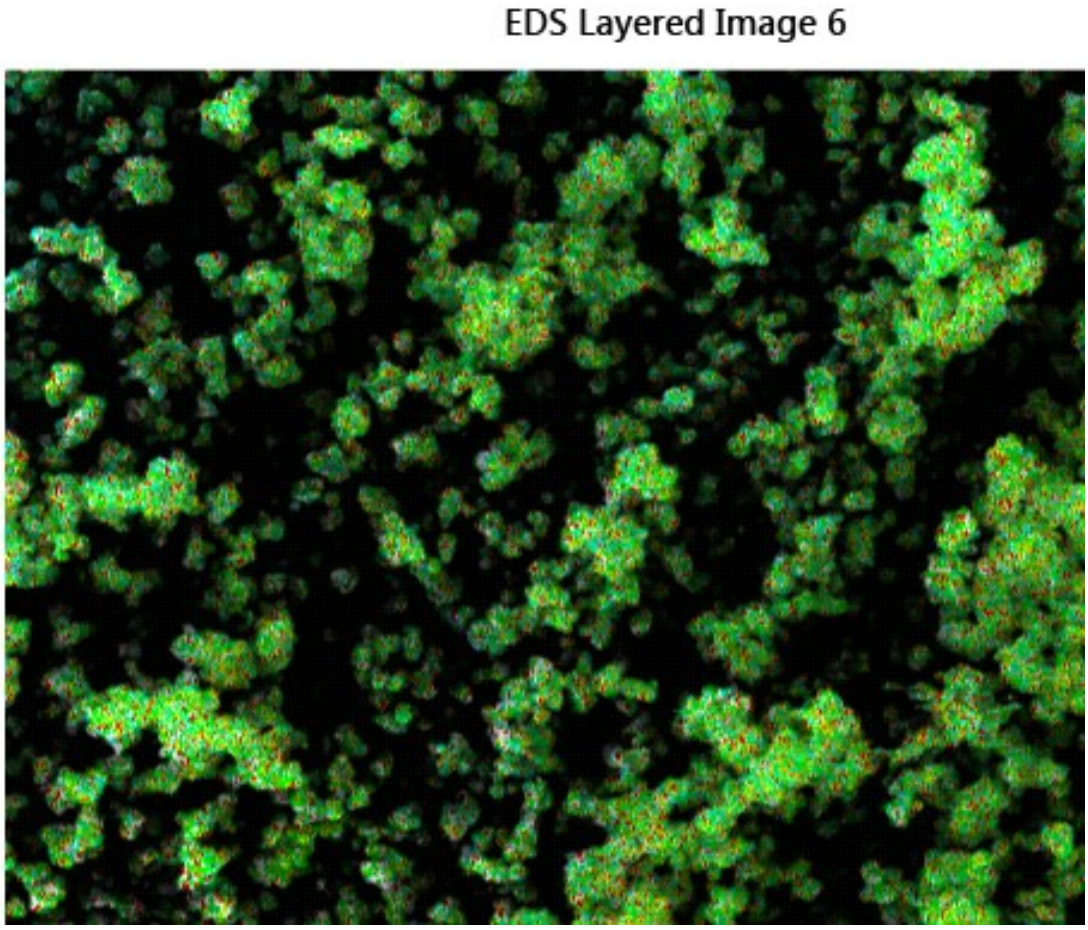

Figure 4.12: Layered 50% Sn site two map

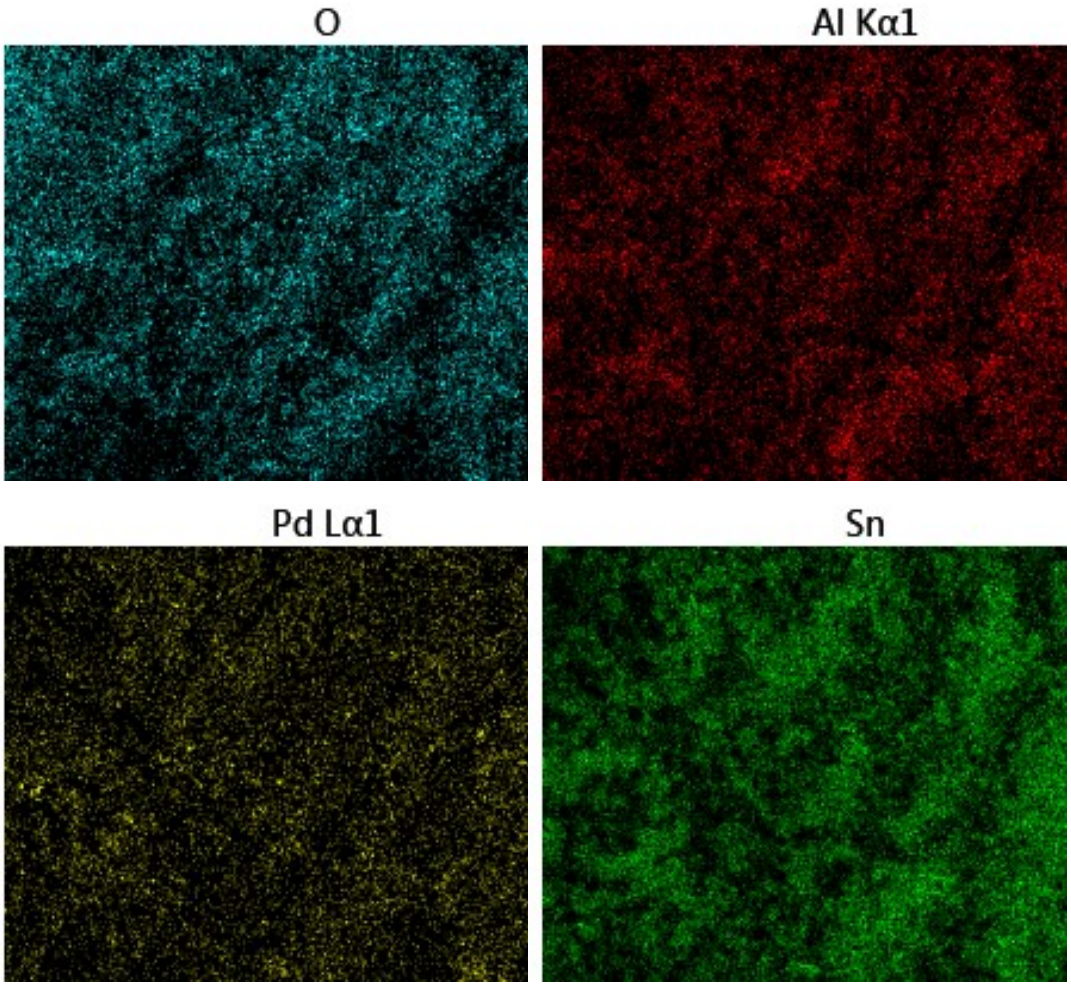

Figure 4.13: Deconvoluted 50 mole % Sn site 2 maps

SEM Imaging

The 10 % Sn support exhibits different morphology to other samples with a mixture of needle-like and elongated flaky particles possessing crevices, creases and jagged edges. These particles vary in length of up to 100 nm with these particles protruding outwards, figure 37. The 50% Sn support has a more spherical morphology with smoother texture and clumped particles starting from 20nm upwards displayed in figure 38). It is possible to see the difference after loading Pd to both samples physically; however, without TEM, it is impossible to see Pd nanoparticles, as they are known to be between 1 nm and 3 nm in size.

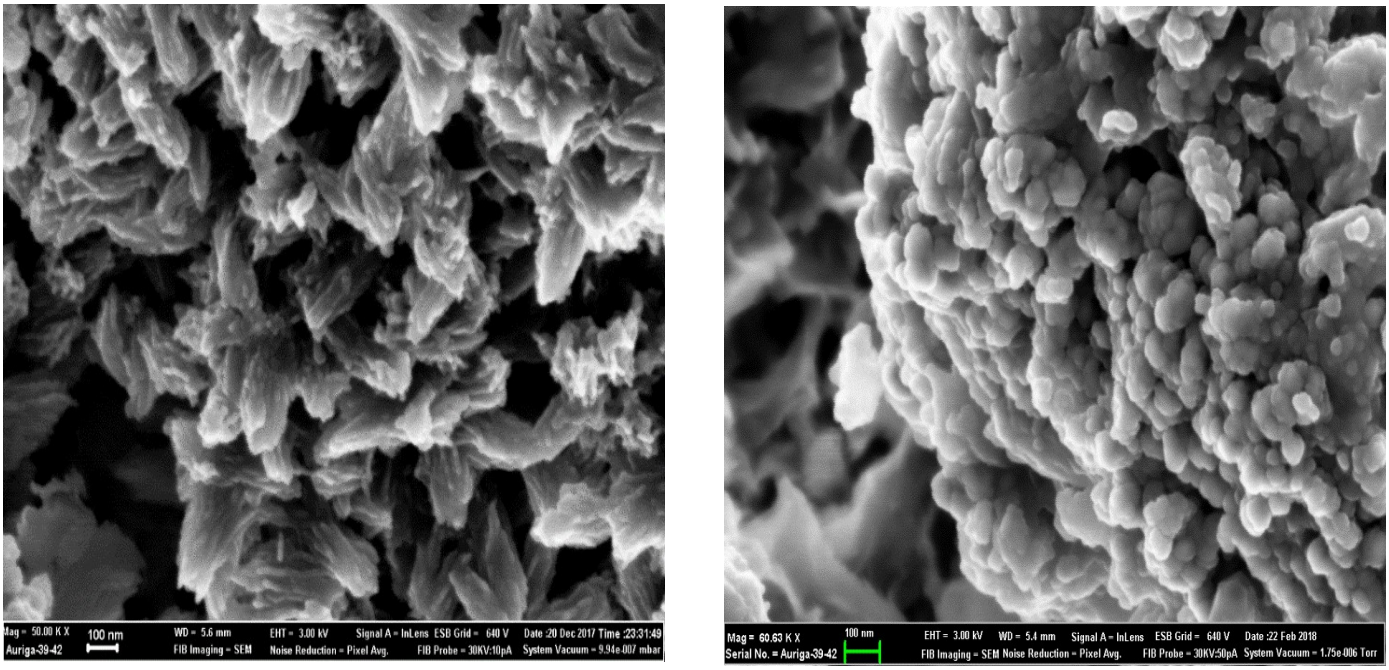

Figure 4.14: 10 % Sn catalyst support material before impregnation (left) and after

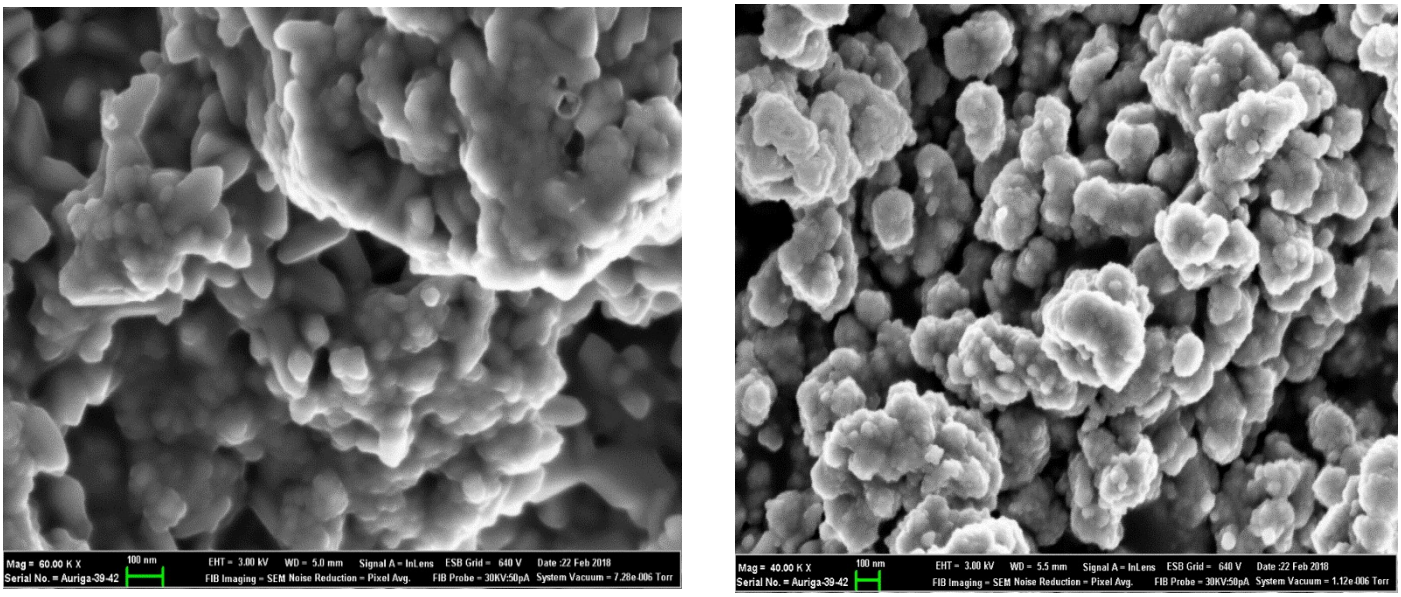

Figure 4.15: 50 % Sn catalyst support material before impregnation (left) and after

XRD

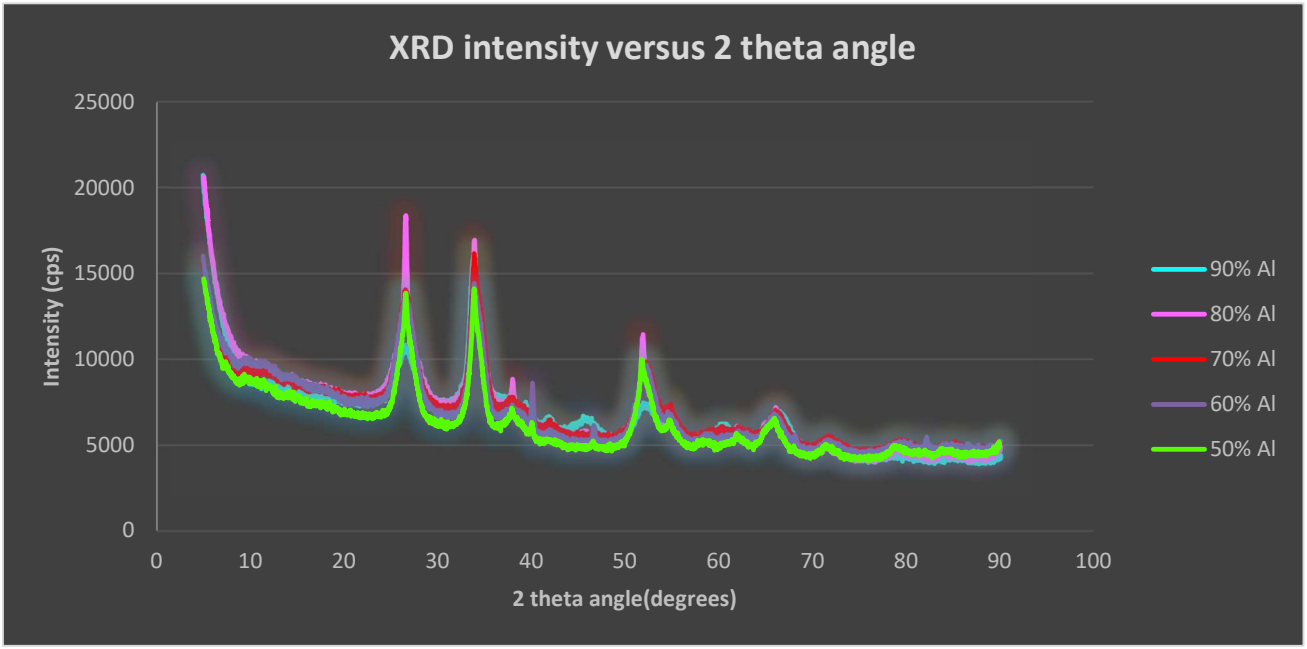

Figure 4.16: XRD results

Table 4.2: XRD reference peak data

XRD reference peaks 2θ angle (degrees)				
Gamma Alumina	**Alpha alumina**	**Tin dioxide**	**Palladium oxide**	**Palladium**
20	25	26	34	40
35	35	34	-	-
40	43	52	-	-
67	58	-	-	-
85	-	-	-	-

XRD crystallography confirmed the formation of both gamma and alpha-alumina phases evidenced by the major reference peaks at 20° and 25°. Gamma alumina oxygen atoms are cubic close-packed with aluminium occupying the octahedral and tetrahedral sites whereas alpha alumina's molecular geometry is hexagonal planar known to be more stable than the gamma phase. Tin dioxide was formed according to reference peak data in the table above with hexagonal molecular geometry. Both Palladium with face centred cubic structure and Palladium oxide, which has tetragonal geometry are present according to the reference peak values. The most crystalline structure was formed with 80% aluminium and least crystalline using 90 % aluminium. 80 % aluminium supported catalyst also exhibits the highest peak intensities for tin dioxide and palladium peaks.

Table 4.3: Process comparison by sustainability analysis

Aspect	Fermentation	Catalysis	Favourable Process
Capital expenditure considerations	Large vessel size is more mostly.	Catalyst expensive (requires regeneration and eventual replacement)	Fermentation
	Large impeller diameter	Large pump required resulting in higher pressure drops	Fermentation
Operational expenditure considerations	Low temp	Low temp	Both
	Mixer work is inefficient power consumption (use airlift reactor)	Pump work is high	Both Unfavourable
Footprint	Larger	Smaller	Catalysis
Production considerations	Batch	Continuous	Both
People	Employs people	Employs people	Both
Planet	Enzymes are cheap biological organisms hence minimum preparation required for this greener process.	Catalyst synthesis involves: 1)Many solvents 2) High temperatures wasting energy 3) Precursor salts are expensive, and the supplier sigma Aldrich also has green issues as the materials are inorganic.	Fermentation

.

CHAPTER 6: CONCLUSIONS AND RECOMMENDATIONS

The gap addressed in the literature review was the use of a composite tin-alumina mixed metal oxide support to improve Lewis acidity. Synthesis of Pd supported catalyst was successful, confirmed by characterisation of five different tin support compositions ranging from 10 mole % tin to 50 mole % tin. The surface area of 90% alumina/10% tin support was desirable at 261,43 m^2/g compared to the surface area of 72.22 m^2/g at 50% tin. The entire composite support surface decreases marginally after impregnation with Pd for all samples as expected due to reduced pore volume. EDX spectra confirm tin, aluminium and Palladium in their elemental form showing that the quantities are close to the nominal amounts. Maps indicate high density in tin even in the 10 % Sn support. Deconvoluted EDX maps display the dispersion. Evenly dispersed palladium nanoparticles are desired over clumped nanoparticles, and one anomaly site displayed a clump, with the others being evenly dispersed. The Pd percentage varies above and below the expected Pd loading but on average will give the expected loading. As per SEM imaging the 10 % Sn support exhibits different morphology to other samples with a mixture of needle-like and elongated flaky particles possessing crevices, creases and jagged edges. These particles vary in length up to 100 nm with particles protruding outwards. The 50% Sn support has a more spherical morphology with smoother texture and clumped particles starting from 20nm upwards displayed in. It is possible to see the difference after loading Pd to both samples physically; however, without TEM, it is impossible to see Pd nanoparticles, as they are known to be between 1 nm and 3 nm in size. XRD crystallography confirmed the formation of both gamma and alpha-alumina phases evidenced by the major reference peaks at 20^o and 25^o. Tin dioxide was also formed according to reference peak data with hexagonal molecular geometry. Both Palladium with face centred cubic structure and Palladium oxide, which has tetragonal geometry are present according to the reference peak values. The most crystalline structure was formed with 80% aluminium and least crystalline using 90 % Aluminium. The 80 % aluminium supported catalyst also exhibits the highest peak intensities for tin dioxide and palladium peaks.

System behaviour should be modelled as an initial screening process before purchasing expensive chemicals such as palladium chloride. Larger vessels should be used when progressing from initial methodology to final methodology as a larger quantity would require larger vessels to maintain catalyst consistency as per the Buckingham pie dimensional analysis. Since Pd is expensive, substitution with a base metal could improve the chemical routes competitiveness. This is achieved by adding stabilizers and promoter dopants to a base metal catalyst impeding the leaching process. Situating production plants production plants close to the harbour will minimise transportation costs as products could be exported from this point. The fermentation process could be enhanced by using co-enzymes and a hybrid fermentation method by depositing suitable metals on the existing enzymes to reduce the batch processing time. An airlift reactor would improve homogeneity during fermentation, requiring less energy as indicated in the sustainability analysis. Raising the sugar tax will assist in xylitol production and deter importers.

REFERENCES

Alen, R. (1999) *Analytical methods in wood chemistry, pulping, and papermaking*. doi: 10.1007/978-3-662-08986-6.

Amarasekara, A. S. and Hasan, M. A. (2015) 'Pd/C catalyzed conversion of levulinic acid to γ-valerolactone using alcohol as a hydrogen donor under microwave conditions'. doi: 10.1016/j.catcom.2014.11.009.

Atkins, P. and Overton, T. (no date) *Inorganic chemistry*. Fifth. ISBN 9781429218207

Augustine, R. L. (1996) *Heterogeneous catalysis for the synthetic chemist*, *Marcel Dekker Inc.ISBN 0824790219*

Barrios, A. M. *et al.* (2018) 'Hydrodeoxygenation of phenol over niobia supported Pd catalyst', *Catalysis Today*. Elsevier, 302(April 2017), pp. 115–124. doi: 10.1016/j.cattod.2017.03.034.

Bhogeswararao, S. and Srinivas, D. (2015) 'Catalytic conversion of furfural to industrial chemicals over supported Pt and Pd catalysts', *Journal of Catalysis*. Elsevier Inc., 327, pp. 65–77. doi: 10.1016/j.jcat.2015.04.018.

Bianca Gumina, Francesco Mauriello, Rosario Pietropaolo, S. G. and Esproa, C. (2018) 'Hydrogenolysis of sorbitol into valuable C3-C2 alcohols at low H2 pressure promoted by the heterogeneous Pd/Fe3O4 catalyst', *Molecular Catalysis*. Elsevier B.V., 446, pp. 152–160. doi: 10.1016/j.mcat.2017.12.038.

Bnfoub, V. O. and Pot, Q. Q. D. B. U. (no date) *Solid acid catalysis*.ISBN 9789814463284

Brieger, G. and Nestrick, T. J. (1973) 'Catalytic Transfer Hydrogenation', 1973.

Castillejos, E. *et al.* (2018) 'When the nature of surface functionalities on modified carbon dominates the dispersion of palladium hydrogenation catalysts', *Catalysis Today*. Elsevier, 301(April 2017), pp. 248–257. doi: 10.1016/j.cattod.2017.05.024.

Cazaña, F. *et al.* (2018) 'Synthesis of Pd-Al/biomorphic carbon catalysts using cellulose as carbon precursor', *Catalysis Today*. Elsevier, 301(May 2017), pp. 226–238. doi: 10.1016/j.cattod.2017.05.026.

Chang, X. *et al.* (2016) 'Catalytic Transfer Hydrogenation of Furfural to 2-Methylfuran and 2-Methyltetrahydrofuran over Bimetallic Copper–Palladium Catalysts', *ChemSusChem*, 9(23), pp. 3330–3337. doi: 10.1002/cssc.201601122.

Chen, B. *et al.* (2015) 'Tuning catalytic selectivity of liquid-phase hydrogenation of furfural via synergistic effects of supported bimetallic catalysts', *Applied Catalysis A: General*. Elsevier B.V., 500, pp. 23–29. doi: 10.1016/j.apcata.2015.05.006.

Chen, J. *et al.* (2015) 'Selective hydrogenation of biomass-based 5-hydroxymethylfurfural over catalyst of palladium immobilized on amine-functionalized metal-organic frameworks', *ACS Catalysis*, 5(2), pp. 722–733. doi: 10.1021/cs5012926.

Chen, J. *et al.* (2017) 'Using palladium catalyst supported on mesoporous graphitic carbon', *Journal of Energy Chemistry*, 14(0), pp. 52–0. doi: 10.1016/j.jechem.2017.04.017.

Dhanalaxmi, K. *et al.* (2017) 'Magnetic nanohybrid decorated porous organic polymer: Synergistic catalyst for high performance levulinic acid hydrogenation', *ACS Sustainable Chemistry and Engineering*, 5(1), pp. 1033–1045. doi: 10.1021/acssuschemeng.6b02338.

Ding, S. *et al.* (2017) 'Pd nanoparticles supported on N-doped porous carbons derived from ZIF-67: Enhanced catalytic performance in phenol hydrogenation', *Journal of Industrial and Engineering Chemistry*. The Korean Society of Industrial and Engineering Chemistry, 46, pp. 258–265. doi: 10.1016/j.jiec.2016.10.037.

Duan, H. *et al.* (2017) 'Hydrodeoxygenation of water-insoluble bio-oil to alkanes using a highly dispersed Pd-Mo catalyst', *Nature Communications*, 8(1). doi: 10.1038/s41467-017-00596-3.

Ebitani, K. (1991) 'Combined temperature programmed reduction -temperature programmed desorption study on supported platinum catalysts', *Bull. chem. Soc. Jpn*. Sapporo, 64(8), pp. 2422–24227.

Entwistle, I. A. N. D. (1985) 'Heterogeneous catalytic transfer hydrogenation and its relation to other methods for reduction of organic compounds', pp. 129–170.

Feng, J., Zhong, Y. H. and Dai, S. H. (2018) 'Hydrogenolysis of α-methylbenzyl alcohol to ethylbenzene over Pd/C catalyst', *IOP Conference Series: Materials Science and Engineering*, 292, p. 012117. doi: 10.1088/1757-899X/292/1/012117.

Fulajtárova, K. *et al.* (2015) 'Aqueous phase hydrogenation of furfural to furfuryl alcohol over Pd–Cu catalysts', *'Applied Catalysis A, General'*, 502, pp. 78–85. doi: 10.1016/j.apcata.2015.05.031.

Garcia-Olmo, A. J. *et al.* (2017) 'Activity of continuous flow synthesized Pd-based nanocatalysts in the flow hydroconversion of furfural'. doi: 10.1016/j.tet.2017.02.056.

Gawade, A. B., Tiwari, M. S. and Yadav, G. D. (2016) 'Biobased green process: Selective hydrogenation of 5-hydroxymethylfurfural to 2,5-dimethyl furan under mild conditions using Pd-Cs2.5H0.5PW12O40/K-10 Clay', *ACS Sustainable Chemistry and Engineering*, 4(8), pp. 4113–4123. doi: 10.1021/acssuschemeng.6b00426.

Gilkey, M. J. and Xu, B. (2016) 'Heterogeneous catalytic transfer hydrogenation as an effective pathway in biomass upgrading', 5(Scheme 1). doi: 10.1021/acscatal.5b02171.

Guo, X. F. *et al.* (2012) 'Hydrogenation and dehydrogenation reactions catalyzed by CNTs supported palladium catalysts', *Catalysis Today*. Elsevier B.V., 186(1), pp. 109–114. doi:

10.1016/j.cattod.2011.11.001.

Hronec, M. *et al.* (2016) 'Carbon supported Pd-Cu catalysts for highly selective rearrangement of furfural to cyclopentanone', *Applied Catalysis B: Environmental*. Elsevier B.V., 181, pp. 210–219. doi: 10.1016/j.apcatb.2015.07.046.

Hu, S. *et al.* (2018) 'Selective hydrogenation of phenol to cyclohexanone over Pd@CN (N-doped porous carbon): Role of catalyst reduction method', *Applied Surface Science*. Elsevier B.V., 435, pp. 649–655. doi: 10.1016/j.apsusc.2017.11.181.

Industry experts (2017) *Xylitol-A global market overview*. URL: Xylitol - A Global Market Overview (prnewswire.com)

Jackson, M. A. *et al.* (2016) 'A one-pot synthesis of 1,6,9,13-tetraoxadispiro(4.2.4.2)tetradecane by hydrodeoxygenation of xylose using a palladium catalyst', *Carbohydrate Research*. Elsevier Ltd, 432, pp. 9–16. doi: 10.1016/j.carres.2016.06.003.

Johnson Matthey, Precious metals management (no date). Available at: http://www.platinum.matthey.com/about-pgm (Accessed: 16 January 2017).

Juszczyk, W. *et al.* (1989) 'Characterization of supported palladium catalysts: III. Pd/Al2O3', *Journal of Catalysis*, 120, pp. 68–77. doi: 10.1016/0021-9517(89)90251-0.

Kim, M. S. *et al.* (2013) 'Catalytic reduction of nitrate in water over Pd-Cu/TiO2 catalyst: Effect of the strong metal-support interaction (SMSI) on the catalytic activity', *Applied Catalysis B: Environmental*. Elsevier B.V., 142–143, pp. 354–361. doi: 10.1016/j.apcatb.2013.05.033.

Larson, R. T. *et al.* (2017) 'Hydrogen gas-mediated deoxydehydration/hydrogenation of sugar acids: catalytic conversion of glucarates to adipates', *Journal of the American Chemical Society*, 139(40), pp. 14001–14004. doi: 10.1021/jacs.7b07801.

Laursen, A. B. *et al.* (2010) 'Substrate size-selective catalysis with zeolite-encapsulated gold nanoparticles', *Angewandte Chemie - International Edition*, 49(20), pp. 3504–3507. doi: 10.1002/anie.200906977.

Lee, J., Kim, Y. T. and Huber, G. W. (2014) 'Aqueous-phase hydrogenation and hydrodeoxygenation of biomass-derived oxygenates with bimetallic catalysts', *Green Chemistry*, 16(2), p. 708. doi: 10.1039/c3gc41071d.

Lesiak, M. *et al.* (2014) 'Hydrogenation of furfural over Pd–Cu/Al 2 O 3 catalysts. The role of interaction between Palladium and copper on determining catalytic properties', *'Journal of Molecular Catalysis. A, Chemical'*, 395, pp. 337–348. doi: 10.1016/j.molcata.2014.08.041.

Li, D. dan, Zhang, J. wei and Cai, C. (2018) 'Chemoselective hydrogenation of nitroarenes catalyzed by cellulose-supported Pd NPs', *Catalysis Communications*. Elsevier, 103(September 2017), pp. 47–50. doi: 10.1016/j.catcom.2017.09.024.

Li, H., Zhao, W. and Fang, Z. (2017) 'Applied catalysis B : environmental hydrophobic Pd nanocatalysts for one-pot and high-yield production of liquid furanic biofuels at low temperatures', 215, pp. 18–27. doi: 10.1016/j.apcatb.2017.05.039.

Li, L. *et al.* (2014) 'Facile fabrication of ultrafine palladium nanoparticles with size- and location-control in click-based porous organic polymers', *ACS Nano*, 8(5), pp. 5352–5364. doi: 10.1021/nn501853g.

Li, L., Zhao, H. and Wang, R. (2015) 'Tailorable synthesis of porous organic polymers decorating ultrafine palladium nanoparticles for hydrogenation of olefins', *ACS Catalysis*, 5(2), pp. 948–955. doi: 10.1021/cs501731w.

Li, M. *et al.* (2018) 'Tuning the selectivity of phenol hydrogenation on Pd/C with acid and basic media', *Catalysis Communications*, 103(June 2017), pp. 88–91. doi: 10.1016/j.catcom.2017.09.028.

Li, S. *et al.* (2015) 'Aqueous-phase hydrogenation of biomass-derived itaconic acid to methyl-γ-butyrolactone over Pd/C catalysts: Effect of pretreatments of active carbon', *CATCOM*, 61, pp. 92–96. doi: 10.1016/j.catcom.2014.12.017.

Li, Z. *et al.* (2013) 'Nitrogen-functionalized ordered mesoporous carbons as multifunctional supports of ultrasmall Pd nanoparticles for hydrogenation of phenol', *ACS Catalysis*, 3(11), pp. 2440–2448. doi: 10.1021/cs400506q.

Liao, F., Lo, T. W. B. and Tsang, S. C. E. (2015) 'Recent developments in palladium-based bimetallic catalysts', *ChemCatChem*, 7(14), pp. 1998–2014. doi: 10.1002/cctc.201500245.

Liao, H. G. *et al.* (2012) 'Hydrogenation of nitrocyclohexane to cyclohexanone oxime over Pd/CNT catalyst under mild conditions', *Catalysis Communications*. Elsevier B.V., 19, pp. 80–84. doi: 10.1016/j.catcom.2011.12.027.

Lieske, H. and Voelter, J. (1985) 'Palladium redispersion by spreading of palladium(II) oxide in oxygen treated palladium/alumina', *The Journal of Physical Chemistry*, 89(10), pp. 1841–1842. doi: 10.1021/j100256a001.

Liu, L., Lou, H. and Chen, M. (2018) 'Selective hydrogenation of furfural over Pt based and Pd based bimetallic catalysts supported on modified multiwalled carbon nanotubes (MWNT)', *Applied Catalysis A: General*. Elsevier, 550(July 2017), pp. 1–10. doi: 10.1016/j.apcata.2017.10.003.

Liu, X. *et al.* (2016) 'A sustainable process for the production of 2-methyl-1,4-butanediol by hydrogenation of biomass-derived itaconic acid', *Catalysis Today*. Elsevier B.V., 274(3), pp. 88–93. doi: 10.1016/j.cattod.2016.01.041.

Luo, W. *et al.* (2015) 'High performing and stable supported nano-alloys for the catalytic hydrogenation of levulinic acid to γ-valerolactone.', *Nature communications*. Nature Publishing Group, 6, p. 6540. doi: 10.1038/ncomms7540.

Luque, R. *et al.* (2009) 'Efficient aqueous hydrogenation of biomass platform molecules using supported metal nanoparticles on Starbons®', *Chemical Communications*, (35), p. 5305. doi: 10.1039/b911877b.

Mai, C. T. Q. and Ng, F. T. T. (2016) 'Effect of metals on the hydrogenolysis of glycerol to higher value sustainable and green chemicals using a supported HSiW Catalyst', *Organic Process Research and Development*, 20(10), pp. 1774–1780. doi: 10.1021/acs.oprd.6b00245.

Mandelli, D. *et al.* (2015) 'Hydrogenolysis of glycerol to alcohols catalyzed by transition metals supported on pillared clay'. doi: 10.1007/s11144-014-0831-y.

Mauriello, F. *et al.* (2015) 'Exploring the catalytic properties of supported palladium catalysts in the transfer hydrogenolysis of glycerol', *Applied Catalysis B: Environmental*. Elsevier B.V., 166–167, pp. 121–131. doi: 10.1016/j.apcatb.2014.11.014.

Meller, E., Sasson, Y. and Aizenshtat, Z. (2016) 'Palladium catalyzed hydrogenation of biomass derived halogenated furfurals', *RSC Adv.*, 6(105), pp. 103149–103159. doi: 10.1039/C6RA21472J.

Minh, D. P. *et al.* (2010) 'Aqueous-phase hydrogenation of biomass-based succinic acid to 1,4-butanediol over supported bimetallic catalysts', *Topics in Catalysis*, 53(15–18), pp. 1270–1273. doi: 10.1007/s11244-010-9580-y.

Mironenko, R. M. *et al.* (2017) 'Liquid-phase hydrogenation of benzaldehyde over Pd-Ru/C catalysts: Synergistic effect between supported metals', *Catalysis Today*. Elsevier B.V., 279, pp. 2–9. doi: 10.1016/j.cattod.2016.07.022.

Musolino, M. G. *et al.* (2011) 'Glycerol hydrogenolysis promoted by supported palladium catalysts', *ChemSusChem*, 4(8), pp. 1143–1150. doi: 10.1002/cssc.201100063.

Nakagawa, Y. *et al.* (2014) 'Total Hydrogenation of Furfural and 5‐Hydroxymethylfurfural over Supported Pd − Ir Alloy Catalyst'.

Nakagawa, Y., Tamura, M. and Tomishige, K. (2017) 'Supported metal catalysts for total hydrogenation of furfural and 5-hydroxymethylfurfural', *Journal of the Japan Petroleum Institute*, 60(1), pp. 1–9. doi: 10.1627/jpi.60.1.

Nakagawa, Y. and Tomishige, K. (2010) 'Total hydrogenation of furan derivatives over silica-supported Ni-Pd alloy catalyst', *Catalysis Communications*. Elsevier B.V., 12(3), pp. 154–156. doi: 10.1016/j.catcom.2010.09.003.

Nishimura, S., Ikeda, N. and Ebitani, K. (2014) 'Selective hydrogenation of biomass-derived 5-hydroxymethylfurfural (HMF) to 2,5-dimethylfuran (DMF) under atmospheric hydrogen pressure over carbon supported PdAu bimetallic catalyst', *Catalysis Today*, 232, pp. 89–98. doi: 10.1016/j.cattod.2013.10.012.

Nishimura, S., Shimura, T. and Ebitani, K. (2017) 'ARTICLE IN PRESS Transfer hydrogenation of

furaldehydes with sodium phosphinate as a hydrogen source using Pd-supported alumina catalyst', *Journal of the Taiwan Institute of Chemical Engineers*, 3(0), pp. 0–1. doi: 10.1016/j.jtice.2017.03.028.

O'Driscoll, Leahy, J. J. and Curtin, T. (2017) 'The influence of metal selection on catalyst activity for the liquid phase hydrogenation of furfural to furfuryl alcohol', *Catalysis Today*. Elsevier B.V., 279, pp. 194–201. doi: 10.1016/j.cattod.2016.06.013.

Ott, L., Bicker, M. and Vogel, H. (2006) 'Catalytic dehydration of glycerol in sub- and supercritical water: a new chemical process for acrolein production', *Green Chem.*, 8(2), pp. 214–220. doi: 10.1039/B506285C.

Otto, K., Haack, L. P. and DeVries, J. E. (1992) 'Identification of two types of oxidized palladium on gamma-alumina by X-ray photoelectron spectroscopy', *Applied Catalysis B, Environmental*, 1(1), pp. 1–12. doi: 10.1016/0926-3373(92)80003-I.

Ouyang, W. *et al.* (2017) 'Towards industrial furfural conversion: Selectivity and stability of palladium and platinum catalysts under continuous flow regime'. doi: 10.1016/j.cattod.2017.07.011.

Rode, C. V (2013) 'Single-Pot Formation of THFAL via catalytic hydrogenation of FFR over Pd/MFI catalyst', *ACS Sustainable Chemistry & Engineering*.

Rogers, S. M. *et al.* (2017) 'Tandem site- and size-controlled Pd nanoparticles for the directed hydrogenation of furfural', *ACS Catalysis*, 7(4), pp. 2266–2274. doi: 10.1021/acscatal.6b03190.

Sandoval, V. H. and Gigola, C. E. (1996) 'Characterization of Pd and Pd-Pb/α-Al2O3 catalysts. A TPR-TPD study', *Applied Catalysis A: General*, 148(1), pp. 81–96. doi: 10.1016/S0926-860X(96)00224-4.

Shi, X. *et al.* (2016) 'Effects of porous oxide layer on performance of Pd-based monolithic catalysts for 2-ethylanthraquinone hydrogenation', *Chinese Journal of Chemical Engineering*. Elsevier B.V., 24(11), pp. 1570–1576. doi: 10.1016/j.cjche.2016.04.032.

Sudhakar, M. *et al.* (2016) 'Vapor phase hydrogenation of aqueous levulinic acid over hydroxyapatite supported metal (M=Pd, Pt, Ru, Cu, Ni) catalysts.', *Applied Catalysis B: Environmental*. Elsevier B.V., 180, pp. 113–120. doi: 10.1016/j.apcatb.2015.05.050.

Supriya, P. *et al.* (2018) 'Biomimetic synthesis of gum acacia mediated Pd-ZnO and Pd-TiO2–Promising nanocatalysts for selective hydrogenation of nitroarenes', *Materials Chemistry and Physics*, 204, pp. 27–36. doi: 10.1016/j.matchemphys.2017.10.026.

Takata, E. *et al.* (2014) 'Production of xylitol and tetrahydrofurfuryl alcohol from xylan in napier grass by a hydrothermal process with phosphorus oxoacids followed by aqueous phase hydrogenation', *Bioresource Technology*, 167, pp. 74–80. doi: 10.1016/j.biortech.2014.05.112.

Testa, M. L. *et al.* (2015) 'Effect of Au on Pd supported over HMS and Ti doped HMS as catalysts for

the hydrogenation of levulinic acid to -valerolactone', *Catalysis Today*, 257, pp. 291–296. doi: 10.1016/j.cattod.2014.06.009.

Townsend, T. M. *et al.* (2017) 'Transfer hydrogenation of aromatic and linear aldehydes catalyzed using Cp * Ir (pyridinesulfonamide) Cl complexes under base-free conditions', *Journal of Organometallic Chemistry*. Elsevier B.V, 843, pp. 7–13. doi: 10.1016/j.jorganchem.2017.05.004.

Tuteja, J. *et al.* (2014) 'Direct synthesis of 1,6-hexanediol from HMF over a heterogeneous Pd/ZrP catalyst using formic acid as hydrogen source', *ChemSusChem*, 7(1), pp. 96–100. doi: 10.1002/cssc.201300832.

Upare, P. P. *et al.* (2011) 'Selective hydrogenation of levulinic acid to ??-valerolactone over carbon-supported noble metal catalysts', *Journal of Industrial and Engineering Chemistry*. The Korean Society of Industrial and Engineering Chemistry, 17(2), pp. 287–292. doi: 10.1016/j.jiec.2011.02.025.

Vaccaro, L. *et al.* (2018) 'Continuous-flow Pd-catalyzed synthesis of cyclohexanones from phenols using sodium formate as a safe hydrogen source', *ChemCatChem*. doi: 10.1002/cctc.201701922.

Vedyagin, A. A., Volodin, A. M., Kenzhin, R. M., Stoyanovskii, V. O., Shubin, Y. V., *et al.* (2017) 'Effect of metal-metal and metal-support interaction on activity and stability of Pd-Rh/alumina in CO oxidation', *Catalysis Today*. Elsevier B.V., 293–294, pp. 73–81. doi: 10.1016/j.cattod.2016.10.010.

Vedyagin, A. A., Volodin, A. M., Kenzhin, R. M., Stoyanovskii, V. O., Rogov, V. A., *et al.* (2017) 'The role of chemisorbed water in formation and stabilization of active sites on Pd/Alumina oxidation catalysts', *Catalysis Today*. Elsevier B.V., pp. 1–9. doi: 10.1016/j.cattod.2017.01.033.

Wang, C. *et al.* (2016) 'Product selectivity controlled by zeolite crystals in biomass hydrogenation over a palladium catalyst', *Journal of the American Chemical Society*, 138(25), pp. 7880–7883. doi: 10.1021/jacs.6b04951.

Xia, Q. *et al.* (2017) 'Selective one-pot production of high-grade diesel-range alkanes from furfural and 2-methylfuran over Pd/NbOPO 4', *ChemSusChem*, 10(4), pp. 747–753. doi: 10.1002/cssc.201601522.

Xiang, Y. Z. *et al.* (2011) 'Selectivity difference between hydrogenation of acetophenone over CNTs and ACs supported Pd catalysts', *Journal of Molecular Catalysis A: Chemical*. Elsevier B.V., 351, pp. 70–75. doi: 10.1016/j.molcata.2011.09.018.

Xu, S. *et al.* (2017) 'Catalytic conversion of cellulose into polyols using carbon-nanotube-supported monometallic Pd and bimetallic Pd–Fe catalysts', *Cellulose*. Springer Netherlands, 24(6), pp. 2403–2413. doi: 10.1007/s10570-017-1275-0.

Yan, K., Lafleur, T., *et al.* (2013) 'Highly selective production of value-added γ-valerolactone from biomass-derived levulinic acid using the robust Pd nanoparticles', *Applied Catalysis A: General*, 468, pp. 52–58. doi: 10.1016/j.apcata.2013.08.037.

Yan, K., Jarvis, C., *et al.* (2013) 'Novel synthesis of Pd nanoparticles for hydrogenation of biomass-derived platform chemicals showing enhanced catalytic performance', *RSC Advances*, 3(48), p. 25865. doi: 10.1039/c3ra43619e.

Yan, K. *et al.* (2014) 'Clean and selective production of γ-valerolactone from biomass-derived levulinic acid catalyzed by recyclable Pd nanoparticle catalyst'. doi: 10.1016/j.jclepro.2014.02.056.

Yan, K., Lafleur, T. and Liao, J. (2013) 'Facile synthesis of palladium nanoparticles supported on multi-walled carbon nanotube for efficient hydrogenation of biomass-derived levulinic acid', *Journal of Nanoparticle Research*, 15(9), pp. 1–7. doi: 10.1007/s11051-013-1906-9.

Yang, G. and Jaakkola, P. (2011) 'Wood chemistry and isolation of extractives from wood', *Literature study for BIOTULI project-Saimaa University of Applied Sciences*, pp. 10–22.

Yang, X. *et al.* (2015) 'Pd nano-particles (NPs) confined in titanate nanotubes (TNTs) for hydrogenation of cinnamaldehyde', *Catalysis Communications*. Elsevier B.V., 59, pp. 184–188. doi: 10.1016/j.catcom.2014.10.031.

Yin, D. *et al.* (2018) 'Highly selective hydrogenation of furfural to tetrahydrofurfuryl alcohol over MIL-101(Cr)-NH 2 supported Pd catalyst at low temperature', *Chinese Journal of Catalysis*. Dalian Institute of Chemical Physics, the Chinese Academy of Sciences, 39(2), pp. 319–326. doi: 10.1016/S1872-2067(18)63009-8.

Zhang, F. *et al.* (2017) 'Efficient production of the liquid fuel 2,5-dimethylfuran from 5-hydroxymethylfurfural in the absence of acid additive over bimetallic PdAu supported on graphitized carbon', *Energy & Fuels*, 31(6), pp. 6364–6373. doi: 10.1021/acs.energyfuels.7b00428.

Zhang, J. *et al.* (2016) 'Zirconium oxide supported palladium nanoparticles as a highly efficient catalyst in the hydrogenation-amination of levulinic acid to pyrrolidones', *ChemCatChem*, pp. 1–8. doi: 10.1002/cctc.201600739.

Zhang, Y. *et al.* (2017a) 'Self-assembled Pd/CeO 2 catalysts by a facile redox approach for high-efficiency hydrogenation of levulinic acid into gamma-valerolactone'. doi: 10.1016/j.catcom.2017.01.008.

Zhang, Y. *et al.* (2017b) 'Self-assembled Pd/CeO 2 catalysts by a facile redox approach for high-efficiency hydrogenation of levulinic acid into gamma-valerolactone'. doi: 10.1016/j.catcom.2017.01.008.

Zhao, Y. (2014) 'Facile synthesis of Pd nanoparticles on SiO2 for hydrogenation of biomass-derived furfural', *Environmental Chemistry Letters*, 12(1), pp. 185–190. doi: 10.1007/s10311-013-0424-4.

Zhou, C.-H. (Clayton) *et al.* (2008) 'Chemoselective catalytic conversion of glycerol as a biorenewable source to valuable commodity chemicals', *Chem. Soc. Rev.*, 37(3), pp. 527–549. doi: 10.1039/B707343G

Appendices

Table 6.1: Analysed catalytic systems

Catalyst	Substrate	Type of reaction	Type of Reactor or process	Reaction Conditions	Process Performance Selectivity=yield/conversion	Reference
Pd/SiO_2 Synthesis in presence of CO2	levulinic acid	H_2 hydrogenation (liquid-phase)	Batch process	180 °C, 90 bar H_2, 6 h,	Conversion (97.3%) Selectivity: (99.2%) γ -valerolactone (GVL)	(Yan, Lafleur, *et al.*, 2013)
PdAu/ Ti(10%)HMS Hexagonal mesoporous silica	levulinic acid	H_2 hydrogenation (liquid-phase)	Batch process	160 °C, 150 bar H_2, 1h, 0.5g catalyst, 150ml 2,5% LA, 1000 rpm	Conversion (100%) Selectivity: (100%) γ -valerolactone (GVL)	(Testa *et al.*, 2015)
Pd(5%)/MCM41	levulinic acid	H_2 hydrogenation (liquid-phase)	Batch process	240 °C, 60 bar H_2, 6 h,	Conversion (100%) Selectivity: (96.3%) γ -valerolactone (GVL)	(Yan *et al.*, 2014)
Pd/C	levulinic acid	Transfer hydrogenation (liquid-phase)	Batch process	Microwave heating 50s Isopropanol/KOH or NaOH	Conversion (86%) Selectivity: (86%) γ -valerolactone (GVL) only product	(Amarasekara and Hasan, 2015)
Pd/CeO2	levulinic acid	H_2 hydrogenation (liquid-phase)	Batch process	Room temp °C, 4 bar H_2, 1.5 h, 2-propanol solvent	Conversion (>99.9%) Selectivity: (100%) γ -valerolactone (GVL)	(Y. Zhang *et al.*, 2017a)
Pd-Cu/ MgO Reduced with formaldehyde 40°C	Furfural	H_2 hydrogenation (liquid-phase)	Batch process	110 °C, 6 bar H_2, 80min,	Conversion (100%) Selectivity: (98.6%) Furfural alcohol	(Fulajtárova *et al.*, 2015)
Pd-Cu/ $Mg(OH)_2$	Furfural	H_2 hydrogenation (liquid-phase)	Batch process	110 °C, 6 bar H_2, 75min,	Conversion (100%) Selectivity: (98.3%) Furfural alcohol	(Fulajtárova *et al.*, 2015)

Reduced with formaldehyde 40°C						
Pd/Al.SBA-15(reduced)	Furfural	H_2 hydrogenation (liquid-phase)	Continuous-flow process	90 °C, 50 bar H_2, 20min= 35s of reaction time due reactor to dead volume	Conversion (91%) Selectivity: (99%) tetrahydrofurfuryl alcohol (THFOL)	(Garcia-Olmo *et al.*, 2017)
Pd/C(commercial)	Furfural	H_2 hydrogenation (liquid-phase)	Continuous-flow process	90 °C, 50 bar H_2, 120min= 210s of reaction time due reactor to dead volume	Conversion (91%) Selectivity: (99%) Furfuryl alcohol	(Garcia-Olmo *et al.*, 2017)
5% Pd/MAGSNC maghemite/silica	Furfural	H_2 hydrogenation (liquid-phase)	Continuous-flow process	150 °C, 50 bar H_2,2h	Conversion (95%) Selectivity: (90%) Furfuryl alcohol	(Ouyang *et al.*, 2017)
5% Pd/MAGSNC maghemite/silica	Furfural	H_2 hydrogenation (liquid-phase)	Continuous-flow process	150 °C, 50 bar H_2, 20min	Conversion (99%) Selectivity: (74%) Furfuryl alcohol	(Ouyang *et al.*, 2017)
Pd/Al_2O_3	Furfural	Transfer hydrogenation (liquid-phase)	Batch process	Room temp 25°C,1h, NaH_2PO_2 / water and THF solvent	Conversion (91%) Selectivity: (64%) Furfuryl alcohol	(Nishimura, Shimura and Ebitani, 2017)
Pd/Al_2O_3	Furfural	Transfer hydrogenation (liquid-phase)	Batch process	Room temp 25°C,1h, $NaBH_4$ / water and THF solvent	Conversion (100%) Selectivity: (87%) Furfuryl alcohol	(Nishimura, Shimura and Ebitani, 2017)
Pd-Cu(1.5%)/ Al_2O_3	Furfural	H_2 hydrogenation (liquid-phase)	Batch process	90 °C, 50 bar H_2, 2h	Conversion (100%) Selectivity: (59%) THFA,(41%) FA	(Lesiak *et al.*, 2014)
Pd-Cu(6%)/ Al_2O_3	Furfural	H_2 hydrogenation (liquid-phase)	Batch process	90 °C, 50 bar H_2, 2h	Conversion (96%) Selectivity: (44%) THFA,(56%) FA	(Lesiak *et al.*, 2014)
Pd/MIL-53(Al)-P	Fructose	Transfer hydrogenation (liquid-phase)	Batch process	110℃,75min, 1atm Donor=polymethylhydrosiloxane (PMHS) /5ml n-BuOH and 6 mol% chlorobenzene	Conversion (99%) Yield: (95%) DMF (2,5-dimethylfuran) Selectivity: (96%) DMF	(Li, Zhao and Fang, 2017)
	Glucose			130℃,120min, 1atm Donor=polymethylhydrosiloxane (PMHS) /5ml n-BuOH and 6 mol% chlorobenzene	Conversion (95%) Yield: (54%) DMF Selectivity: (57%) DMF	
	Sucrose			110℃,150min, 1atm Donor=polymethylhydrosiloxane (PMHS) /5ml n-BuOH and 6 mol% chlorobenzene	Conversion (100%) Selectivity: (73%) DMF	

Pd/MIL-53(Al)-P	Inulin	Transfer hydrogenation (liquid-phase	Batch process	110℃,150min, 1atm Donor=polymethylhydrosiloxane (PMHS) /5ml n-BuOH and 6 mol% chlorobenzene	Conversion (97%) Yield: (86%) DMF Selectivity: (89%) DMF	(Li, Zhao and Fang, 2017)
	Xylose			130℃,120min, 1atm Donor=polymethylhydrosiloxane (PMHS) /5ml n-BuOH and 6 mol% chlorobenzene	Conversion (93%) Yield: (45%) MF (2-methylfuran) Selectivity: (48%) MF	
	HMF			25℃,150min, 1atm Donor=polymethylhydrosiloxane (PMHS) /5ml n-BuOH and 6 mol% chlorobenzene	Conversion (100%) Selectivity: (99%) DMF	
	5-Methyl furfural			25℃,120min, 1atm Donor=polymethylhydrosiloxane (PMHS) /5ml n-BuOH and 6 mol% chlorobenzene	Conversion (100%) Selectivity: (99%) DMF	
	5-Methyl furfuryl alcohol			25℃,90min, 1atm Donor=polymethylhydrosiloxane (PMHS) /5ml n-BuOH and 6 mol% chlorobenzene	Conversion (99%) Yield: (98%) DMF Selectivity: (99%) DMF	
	Furfural			25℃,120min, 1atm Donor=polymethylhydrosiloxane (PMHS) /5ml n-BuOH and 6 mol% chlorobenzene	Conversion (100%) Selectivity: (97%) MF	
	Furfuryl alcohol			25℃,90min, 1atm Donor=polymethylhydrosiloxane (PMHS) /5ml n-BuOH and 6 mol% chlorobenzene	Conversion (98%) Yield: (96%) MF Selectivity: (98%) MF	
	Benzaldehyde			25℃,120min, 1atm Donor=polymethylhydrosiloxane (PMHS) /5ml n-BuOH and 6 mol% chlorobenzene	Conversion (100%) Selectivity: (97%) toluene	
Pd/MIL-53(Al)-P	Acetophenone	Transfer hydrogenation (liquid-phase)	Batch process	25℃,120min, 1atm Donor=polymethylhydrosiloxane (PMHS) /5ml n-BuOH and 6 mol% chlorobenzene	Conversion (99%) Yield: (95%) Ethylbenzene Selectivity: (96%) Ethylbenzene	(Li, Zhao and Fang, 2017)
Pd/mpg-C_3N_4 (4.1wt%)		H_2 hydrogenation			Conversion (>99%) Selectivity: (97%) DHMTHF	(Chen *et al.*, 2017)

mesoporous graphitic carbon nitride Pd/mpg-C3N4 (1.2wt%)	5-hydroxymethylfurfural (HMF)	(liquid-phase)	Batch process	60°C, 10 bar H_2, 4h	2,5-dihydroxymethyl-tetrahydrofuran Conversion (>99%) Selectivity: (68%) DHMTHF, 30%DHMF(dihydroxymethylfuran)	
Pd-Au/C	HMF	H2 hydrogenation (liquid-phase)	Batch process	60°C, 1atm H_2, 12h	Conversion (>99%) Selectivity: (>99%) DHF 2,5-dimethylfuran	(Nishimura, Ikeda and Ebitani, 2014)
Pd/C	Xylose	H2 hydrogenation (liquid-phase)	Batch process	135°C, 50bar H_2, 1h	Conversion (100%) Selectivity: (73.5%) Xylitol	(Takata *et al.*, 2014)
	Furfural			150°C, 50bar H_2, 1h	Conversion (100%) Selectivity: (79.6%) THFA	
Pd/C pre-treated with HNO_3 and NaClO	Itaconic acid	H2 hydrogenation (liquid-phase)	Batch process	180°C, 40bar H_2, 20h	Conversion (100%) Selectivity: (89.5%) methyl-γ-butyrolactone	(Li *et al.*, 2015)
Pd-Au/C GC800 (graphitized carbon)	HMF	H2 hydrogenation (liquid-phase)	Batch process	150°C, 10bar H_2, 4h	Conversion (86,8%) Selectivity: (94.4%) DMF	(F. Zhang *et al.*, 2017)
Pd/TiO_2	Furfural	H2 hydrogenation (liquid-phase)	Batch process	50°C, 5bar H_2, 15min	Conversion (10%) Selectivity: (78%)FA	(Rogers *et al.*, 2017)
$Pd-Ni/SiO_2$	HMF	H2 hydrogenation (liquid-phase)	Batch process	40°C, 80bar H_2, 2h	Yield=96%BHTHF 2,5-bis(hydroxymethyl)tetrahydrofuran (BHTHF), Selectivity not mentioned	(Nakagawa, Tamura and Tomishige, 2017)
$Pd/NbOPO_4$	Furfural and 2-methylfuran	H2 hydrogenation (liquid-phase)	Batch process	80°C, 5h HAA reaction 200°C, 40bar H_2,12h HDO reaction	One pot process overall yield= 89.1% diesel range alkanes	(Xia *et al.*, 2017)
$Pd-Cu/ZrO_2$	Furfural	Transfer hydrogenation (liquid-phase)	Batch process	220°C, 4h 2-propanol donor	Conversion (100%) Selectivity: 2-MF(61.9%), 2-MTHF (20.4%)	(Chang *et al.*, 2016)
$Pd-Cu/Al_2O_3$	Furfural	Transfer hydrogenation (liquid-phase)	Batch process	220°C, 4h 2-propanol donor	Conversion (100%) Selectivity: 2-MF(32.3%), 2-MTHF (26.2%)	
Pd-Cu/SiO2	Furfural	Transfer hydrogenation (liquid-phase)	Batch process	220°C, 4h 2-propanol donor	Conversion (100%) Selectivity: 2-MF (35.2%), 2-MTHF (24.4%)	

Pd-Cu/TiO2	Furfural	Transfer hydrogenation (liquid-phase)	Batch process	220°C, 4h 2-propanol donor	Conversion (100%) Selectivity: 2-MF (61%), 2-MTHF (5.6%)	
Pd-$Cs_{2.5}H_{0.5}PW_{12}O_{40}$/K-10 clay (palladium-Cesium dodecatungstophosphoric acid supported on K-10 acidic clay)	HMF	H2 hydrogenation (liquid-phase)	Batch process	90°C, 10 atm H_2, 2h	Conversion (98%) Selectivity: 2.5-DMF (81%),	(Gawade, Tiwari and Yadav, 2016)
Pd@S-1 (Silicate-I zeolite crystals core shell structure)	Furfural	H2 hydrogenation (liquid-phase)	Continuous-flow process	250°C, 1atm (system pressure) 10% H_2 /Ar 10 ml/min, 0.5ml/hr Feed rate	Conversion (91.3%) Selectivity: Furan (98.7%),	(Wang *et al.*, 2016)
Pd-Cu/C	Furfural	H2 hydrogenation (liquid-phase)	Batch process	160°C, 30bar H_2, 1h	Conversion (98%) Selectivity: Cyclopentanone (92.1%),	(Hronec *et al.*, 2016)
Pd/C	CMF 5-chloromethyl furfural	H2 hydrogenation (liquid-phase)	Batch process	70°C, 11bar H_2, 1h	Conversion (100%) Selectivity: MF (5-methyl furfural) (99%),	(Meller, Sasson and Aizenshtat, 2016)
Pd/C	BMF 5-bromomethyl furfural	H2 hydrogenation (liquid-phase)	Batch process	50°C, 11bar H_2, 1h	Conversion (100%) Selectivity: MF (5-methyl furfural) (98%),	
Pd/Al_2O_3	Furfural	H2 hydrogenation (liquid-phase)	Batch process	25°C, 60bar H_2, 8h	Conversion (80.3%) Selectivity: THFOL tetrahydrofurfuryl alcohol (97.4%),	(Bhogeswararao and Srinivas, 2015)
Pd/MIL-101(Al)-NH_2 (Metal organic framework)	HMF	H2 hydrogenation (liquid-phase)	Batch process	30°C, 10bar H_2, 12h	Conversion (100%) Selectivity: DHMTHF 2,5-dihydroxymethyl-tetrahydrofuran (96%),	(J. Chen *et al.*, 2015)
Pd/TiO_2–ZrO_2	Furfural	H2 hydrogenation (liquid-phase)	Batch process	130°C, 50bar H_2, 8h	Conversion (98.5%) Selectivity: THFA tetrahydrofurfuryl alcohol (80%),	(B. Chen *et al.*, 2015)
Ni-Pd/TiO_2–ZrO_2	Furfural	H2 hydrogenation (liquid-phase)	Batch process	130°C, 50bar H_2, 8h	Conversion (100%) Selectivity: THFA (59.8%), FA:39.1%	
Ni-Pd	Furfural	H2 hydrogenation (liquid-phase)	Batch process	130°C, 50bar H_2, 8h	Conversion (99.4%) Selectivity: THFA (93.4%), FA:2.1%	

Pd/SiO_2	Furfural	H2 hydrogenation (liquid-phase)	Batch process	Mild conditions stated with no values	Conversion (75%) Selectivity: THFA (18.1%), FA:70.9%	(Zhao, 2014)
Pd/MFI (silica molecular sieve)	Furfural	H2 hydrogenation (liquid-phase)	Batch process	220°C, 34.5bar H_2, 5h	Conversion (84%) Selectivity: THFA (99%),	(Rode, 2013)
Pd-Cu/MFI	Furfural	H2 hydrogenation (liquid-phase)	Batch process	220°C, 34.5bar H_2, 5h	Conversion (100%) Selectivity: FA (91%),	
Pd/SiO_2	Furfural	H2 hydrogenation (liquid-phase)	Batch process	220°C, 34.5bar H_2, 5h	Conversion (76%) Selectivity: FA (50%), THFA (31%),	(Rode, 2013)
$Pd\text{-}Ir/SiO_2$	Furfural	H2 hydrogenation (liquid-phase)	Batch process	2°C, 80bar H_2, 6h	Conversion (99%) Selectivity: THFA (94%),	(Nakagawa *et al.*, 2014)
Pd/ZrP	HMF	Transfer hydrogenation (liquid-phase)	Batch process	140°C, 21h Formic acid as donor/ethanol	Conversion (92.5%) Selectivity: HDO (37.8%), HDN(15.2%), THFDM (12.1%)	(Tuteja *et al.*, 2014)
Pd/Nb_2O_5	HMF	Transfer hydrogenation (liquid-phase)	Batch process	140°C, 21h Formic acid as donor/ethanol	Conversion (93.3%) Selectivity: HDO (20.7%), HDN(12.3%),	
Pd/ZrO_2	levulinic acid	H2 hydrogenation (liquid-phase)	Batch process	90°C, 5bar H_2, 12h	Conversion (100%) Selectivity: 5-methyl-1-octylpyrrolidin-2-one) (98.7%)	(Zhang *et al.*, 2016)
Pd/Al_2O_3	levulinic acid	H2 hydrogenation (liquid-phase)	Batch process	90°C, 5bar H_2, 12h	Conversion (76.1%) Selectivity: 5-methyl-1-octylpyrrolidin-2-one) (87%)	
Pd/PPTPA-1 (Nanoporous polytriphenylamine - Porous organic polymer)	levulinic acid	Transfer hydrogenation (liquid-phase)	Batch process	120°C, 12h Formic acid as donor/ethanol solvent	Conversion (63%) Selectivity: GVL(72%)	(Dhanalaxmi *et al.*, 2017)
Pd-Fe/PPTPA-1	levulinic acid	Transfer hydrogenation (liquid-phase)	Batch process	140°C, 12h Formic acid as donor/ethanol	Conversion (96%) Selectivity: GVL(94%)	
$Pd\text{-}Fe_3O_4$	levulinic acid	Transfer hydrogenation (liquid-phase)	Batch process	140°C, 12h Formic acid as donor/ethanol solvent	Conversion (46%) Selectivity: GVL(83%)	

Pd-Fe_3O_4/PPTPA-1	levulinic acid	Transfer hydrogenation (liquid-phase)	Batch process	120°C, 12h isopropanol as donor	Conversion (65%) Selectivity: GVL(99%)	
Pd-Fe_3O_4/PPTPA-1	levulinic acid	Transfer hydrogenation (liquid-phase)	Batch process	120°C, 12h Ammonium formate as donor	Conversion (55%) Selectivity: GVL(75%)	(Dhanalaxmi *et al.*, 2017)
Pd-HAP Hydroxyapatite crystals	levulinic acid	H2 hydrogenation (liquid-phase)	Continuous-flow process	275°C, H_2 20ml/min, LA feed rate=1-2ml/hr	Conversion (25.3%) Selectivity: GVL(66.5%)	(Sudhakar *et al.*, 2016)
Ru-Pd/TiO_2	levulinic acid	H2 hydrogenation (liquid-phase)	Batch process	200°C, 40bar H_2, 30min	Conversion (>99%) Selectivity: GVL (99.6%)	(Luo *et al.*, 2015)
Au-Pd/TiO_2	levulinic acid	H2 hydrogenation (liquid-phase)	Batch process	200°C, 40bar H_2, 5h	Conversion (90%) Selectivity: GVL (97.3%)	
Pd/CNT Carbon nanotube	levulinic acid	H2 hydrogenation (liquid-phase)	Batch process	200°C, 60bar H_2, 6h	Conversion (57.6%) Selectivity: GVL (97.7%)	(Yan, Lafleur and Liao, 2013)
Pd/C	levulinic acid	H2 hydrogenation (gas-phase)	Continuous-flow process	265°C, 1bar H_2	Conversion (100%) Selectivity: GVL (90%)	(Upare *et al.*, 2011)
Pd-Fe/CNT Carbon nanotube	Cellulose	H2 hydrogenation (liquid phase)	Batch process	240°C, 40bar H_2, 2h	Conversion (100%) Selectivity: Polyols (55%) (hexitol, ethylene glycol, propanediol, glycerol)	(Xu *et al.*, 2017)
Pd//HSiW/Al_2O_3 Where HSiW is silicotungstic acid	Glycerol	H2 hydrogenation (liquid phase)	Batch process	240°C, 60.67bar H_2, 8h	Conversion (34.1%) Selectivity: 1-propanol (51.4%)	(Mai and Ng, 2016)
Pd/Al-Pilc montmorillonite aluminium pillared clay	Glycerol	H2 hydrogenation (liquid phase)	Batch process	120°C, 50bar H_2, 10h	Conversion (2.1%) Selectivity: 1-propanol (95%)	(Mandelli *et al.*, 2015)
Pd/Co_3O_4 Co-precipitation	Glycerol	Transfer hydrogenolysis (liquid phase)	Batch process	180°C, 5bar N_2, 24h 2-propanol as donor and solvent	Conversion (100%) Selectivity: 1.2-PDO: 1.2 propanediol (95%) EG (8.2%) 1-PO(24.9%)	(Mauriello *et al.*, 2015)
Pd/Co_3O_4 Impregnation	Glycerol	Transfer hydrogenolysis (liquid phase)	Batch process	180°C, 5bar N_2, 24h 2-propanol as donor and solvent	Conversion (37.9%) Selectivity: 1.2-PDO (14.6%) EG (6.1%) AC-hydroxyacetone (37.4%)	(Mauriello *et al.*, 2015)

Pd/Fe_3O_4 Co-precipitation	Glycerol	Transfer hydrogenolysis (liquid phase)	Batch process	180°C, 5bar N_2, 24h 2-propanol as donor and solvent	Conversion (100%) Selectivity: 1.2-PDO (55.9%) EG (1.8%) AC (25.2%)	
Pd/Fe_3O_4 Impregnation	Glycerol	Transfer hydrogenolysis (liquid phase)	Batch process	180°C, 5bar N_2, 24h 2-propanol as donor and solvent	Conversion (66.5%) Selectivity: 1.2-PDO (47.7%) EG (8%) AC (43.3%)	
Pd/Fe_2O_3	Glycerol	Transfer hydrogenolysis (liquid phase)	Batch process	180°C, 5bar N_2, 24h 2-propanol as donor and solvent	Conversion (40.4%) Selectivity: 1.2-PDO (26.6%) EG (6.6%) AC(58.1%)	
Pd/CoO	Glycerol	H2 hydrogenolysis (liquid phase)	Batch process	180°C, 5bar H_2, 24h 2-propanol as solvent	Conversion (100%) Selectivity: 1.2-PDO (10.2%) EG (1.9%) 1-propanol(80.9%)	(Musolino *et al.*, 2011)
Pd/Fe2O3	Glycerol	H2 hydrogenolysis (liquid phase)	Batch process	180°C, 5bar H_2, 24h 2-propanol as solvent	Conversion (100%) Selectivity: 1.2-PDO (71.2%), EG (3.4%), 1-propanol(24.5%)	
Pd/ZnO	Glycerol	H2 hydrogenolysis (liquid phase)	Batch process	180°C, 5bar H_2, 24h 2-propanol as solvent	Conversion (93.6%) Selectivity: 1.2-PDO (59.2%), 1-propanol(3.3%), AC(19.4%)	
Pd/NiO	Glycerol	H2 hydrogenolysis (liquid phase)	Batch process	180°C, 5bar H_2, 24h 2-propanol as solvent	Conversion (90.1%) Selectivity: 1.2-PDO (84.1%), EG(10.1%)	(Musolino *et al.*, 2011)
Pd/CoO unreduced	Glycerol	H2 hydrogenolysis (liquid phase)	Batch process	180°C, 5bar H_2, 24h dioxane as solvent	Conversion (100%) Selectivity: 1.2-PDO (60%) 1-propanol (30.5%)	

Pd/Fe2O3 unreduced	Glycerol	H2 hydrogenolysis (liquid phase)	Batch process	180°C, 5bar H_2, 24h dioxane as solvent	Conversion (100%) Selectivity: 1.2-PDO (72.4%), 1-propanol(22.9%)	
Pd/ZnO	Glycerol	H2 hydrogenolysis (liquid phase)	Batch process	180°C, 5bar H_2, 24h dioxane as solvent	Conversion (66.1%) Selectivity: 1.2-PDO (97.7%),	
Pd/NiO	Glycerol	H2 hydrogenolysis (liquid phase)	Batch process	180°C, 5bar H_2, 24h dioxane as solvent	Conversion (80.1%) Selectivity: 1.2-PDO (79.5%), EG(13.3%)	
Pd/AC(activated carbon)	Acetophenone	H2 hydrogenolysis (liquid phase)	Batch process	60°C, 1atm H_2, 10min	Conversion (20%) Selectivity: α-phenylethanol (71%)	(Xiang *et al.*, 2011)
Pd/AC(activated carbon)	Acetophenone	H2 hydrogenolysis (liquid phase)	Batch process	60°C, 1atm H_2, 2h	Conversion (95%) Selectivity: α-phenylethanol (25%)	
Pd/CNT (carbon nanotubes)	Acetophenone	H2 hydrogenolysis (liquid phase)	Batch process	60°C, 1atm H_2, 4h	Conversion (95.3%) Selectivity: α-phenylethanol (96.5%)	
Pd/CNT (carbon nanotubes)	nitro cyclohexane	H2 hydrogenation (liquid phase)	Batch process	50°C, 2bar H_2, 6h	Conversion (97.6%) Selectivity: cyclohexanone oxime (85.9 %)	(Liao *et al.*, 2012)
Pd/CNT (carbon nanotubes)	Benzaldehyde	H2 hydrogenation (liquid phase)	Continuous flow process	100°C, 30ml H_2/min, 3ml/hr feed	Conversion (100%) Selectivity: BA Benzyl alcohol (4.7%) TOL Toluene (94.4%) MC Methylcyclohexane (0.9%)	(Guo *et al.*, 2012)
Pd/CNT (carbon nanotubes)	Benzaldehyde	H2 hydrogenation (liquid phase)	Continuous flow process	200°C, 30ml H_2/min, 3ml/hr feed	Conversion (97.8%) Selectivity: BA Benzyl alcohol (38.6%) TOL toluene (44.1%) MC Methylcyclohexane (17.3%)	
Pd/CNT (carbon nanotubes)	Benzaldehyde	H2 hydrogenation (liquid phase)	Continuous flow process	300°C, 30ml H_2/min, 3ml/hr feed	Conversion (99.5%) Selectivity: BA Benzyl alcohol (0%) TOL Toluene (12.9%) MC Methylcyclohexane (87.1%)	(Guo *et al.*, 2012)
Pd/SiO_2	Benzaldehyde	H2 hydrogenation (liquid phase)	Continuous flow process	100°C, 30ml H_2/min, 3ml/hr feed	Conversion (70.3%) Selectivity: BA Benzyl alcohol (88.4%)	

					TOL Toluene (11.6%) MC Methylcyclohexane (0%)	
Pd/SiO_2	Benzaldehyde	H2 hydrogenation (liquid phase)	Continuous flow process	200°C, 30ml H_2/min, 3ml/hr feed	Conversion (80.5%) Selectivity: BA Benzyl alcohol (90.5%) TOL Toluene (9.5%) MC Methylcyclohexane (0%)	
Pd/SiO_2	Benzaldehyde	H2 hydrogenation (liquid phase)	Continuous flow process	300°C, 30ml H_2/min, 3ml/hr feed	Conversion (5.2%) Selectivity: BA Benzyl alcohol (37.6%) TOL Toluene (3.4%) MC Methylcyclohexane (59%)	
Pd/Al_2O_3	Benzaldehyde	H2 hydrogenation (liquid phase)	Continuous flow process	100°C, 30ml H_2/min, 3ml/hr feed	Conversion (15%) Selectivity: BA Benzyl alcohol (92.9%) TOL Toluene (7.1%) MC Methylcyclohexane (0%)	
Pd/Al_2O_3	Benzaldehyde	H2 hydrogenation (liquid phase)	Continuous flow process	200°C, 30ml H_2/min, 3ml/hr feed	Conversion (30%) Selectivity: BA Benzyl alcohol (96.6%) TOL Toluene (3.4%) MC Methylcyclohexane (0%)	
Pd/Al_2O_3	Benzaldehyde	H2 hydrogenation (liquid phase)	Continuous flow process	300°C, 30ml H_2/min, 3ml/hr feed	Conversion (5.3%) Selectivity: BA Benzyl alcohol (19.1%) TOL Toluene (4.5%) MC Methylcyclohexane (76.4%)	
Pd/NGC (Nanoglobular carbon)	Benzaldehyde	H2 hydrogenation (liquid phase)	Batch process	40°C, 5bar H_2, 5h	Conversion (99.3%) Selectivity: BA Benzyl alcohol (41.9%) TOL Toluene (52%)	(Mironenko *et al.*, 2017)
Pd-Ru/NGC (Nanoglobular carbon)	Benzaldehyde	H2 hydrogenation (liquid phase)	Batch process	40°C, 5bar H_2, 5h	Conversion (100%) Selectivity: BA Benzyl alcohol (89.6%) TOL Toluene (7.6%)	
Pd/CNT (carbon nanotube)	Benzaldehyde	H2 hydrogenation (liquid phase)	Batch process	40°C, 5bar H_2, 5h	Conversion (31.6%)	(Mironenko *et al.*, 2017)

					Selectivity: BA Benzyl alcohol (82.8%) TOL Toluene (0.8%)	
Pd-Ru/CNT (carbon nanotube)	Benzaldehyde	H2 hydrogenation (liquid phase)	Batch process	40°C, 5bar H_2, 5h	Conversion (100%) Selectivity: BA Benzyl alcohol (57.4%) TOL Toluene (39.7%)	
Pd@CPP-C (1,2,3-triazolyl-containing porous organic polymers)	1-hexene	H2 hydrogenation (liquid phase)	Batch process	25°C, 1atm H_2, 1.5h	Conversion (100%) Selectivity: n-hexane (100%)	(Li, Zhao and Wang, 2015)
Pd@CPP-Y (1,2,3-triazolyl-containing porous organic polymer)	1-hexene	H2 hydrogenation (liquid phase)	Batch process	25°C, 1atm H_2, 1h	Conversion (100%) Selectivity: n-hexane (100%)	
Pd@CPP-Y (1,2,3-triazolyl-containing porous organic polymers)	Styrene	H2 hydrogenation (liquid phase)	Batch process	25°C, 1atm H_2, 30min	Conversion (100%) Selectivity: ethyl benzene (100%)	
Pd@CPP-1 click-based porous organic polymers, 1,2,3-triazolyl	Nitrobenzene	H2 hydrogenation (liquid phase)	Batch process	25°C, 1atm H_2, 45min Ethanol solvent	Conversion (100%) Selectivity: aniline (100%)	(Li *et al.*, 2014)
Pd@CPP-2 click-based porous organic polymers, 1,2,3-triazolyl	Nitrobenzene	H2 hydrogenation (liquid phase)	Batch process	25°C, 1atm H_2, 20min Ethanol solvent	Conversion (100%) Selectivity: aniline (100%)	
$Pd^{2.5}$@FDU^{3}-N^{H} N-doped mesoporous carbon	Phenol	H2 hydrogenation (liquid phase)	Batch process	30°C, 1atm H_2, 24h	Conversion (85%) Selectivity: Cyclohexanone (>98%)	(Li *et al.*, 2013)
Pd^{5}@FDU^{3}-N^{H} N-doped mesoporous carbon	Phenol	H2 hydrogenation (liquid phase)	Batch process	100°C, 1 bar H_2, 1h	Conversion (80%) Selectivity: Cyclohexanone (>99%)	
Pd@CN_{550} N-doped mesoporous carbon	Phenol	H2 hydrogenation (liquid phase)	Batch process	80°C, 1 bar H_2, 2h	Conversion (48.9%) Selectivity: Cyclohexanone (99.1%)	(Ding *et al.*, 2017)
Pd@CN_{700}	Phenol	H2 hydrogenation	Batch process	80°C, 1 bar H_2, 2h	Conversion (86%)	

N-doped mesoporous carbon		(liquid phase)			Selectivity: Cyclohexanone (90.3%)	
Pd@CN_{600} N-doped mesoporous carbon with higher Pd content (3.51%)	Phenol	H2 hydrogenation (liquid phase)	Batch process	80°C, 1 bar H_2, 95 min	Conversion (95.6%) Selectivity: Cyclohexanone (94.9%)	
Pd@TNT Titania nanotubes	Cinnamaldehyde	H2 hydrogenation (liquid phase)	Batch process	30°C, 5 bar H_2, 7h 5 min	Conversion (~100%) Selectivity: hydrocinnamaldehyde (~80%)	(Yang *et al.*, 2015)
Pd/C Activated carbon	Itaconic acid	H2 hydrogenation (liquid-phase)	Batch process	180°C, 40bar H_2, 6h	Conversion (100%) Selectivity: (41.6%) 2-MGBL methyl-γ-butyrolactone (55.2%) 3-MGBL	(Liu *et al.*, 2016)
Pd–3ReO_x/C	Itaconic acid	H2 hydrogenation (liquid-phase)	Batch process	180°C, 40bar H_2, 2h	Conversion (100%) Selectivity: (31.7%) 2-MGBL (47.3%) 3-MGBL	
Pd–3ReO_x/C	Itaconic acid	H2 hydrogenation (liquid-phase)	Batch process	180°C, 40bar H_2, 6h	Conversion (100%) Selectivity: (81.2%)MBDO: 2-methyl-1,4-butanediol	
Pd–9ReO_x/C	Itaconic acid	H2 hydrogenation (liquid-phase)	Batch process	180°C, 40bar H_2, 2h	Conversion (100%) Selectivity: (15.6%) 2-MGBL (24.3%) 3-MGBL (55.9%)MBDO	(Liu *et al.*, 2016)
Pd/C	2-methyl-γ-butyrolactone	H2 hydrogenation (liquid-phase)	Batch process	180°C, 40bar H_2, 2h	Conversion (75.2%) Selectivity: (90.3%) MBDO	
Pd–3ReO_x/C	2-methyl-γ-butyrolactone	H2 hydrogenation (liquid-phase)	Batch process	180°C, 40bar H_2, 2h	Conversion (8.1%) Selectivity: (86.5%) MBDO	
Pd/Fe_3O_4	Sorbitol	H2 hydrogenolysis (liquid-phase	Batch process	240°C, 5bar H_2, 24h	Conversion (100%) Selectivity: (63.5%) Ethanol (5.9%) 1,2 propandiol (13%) 1-propanol	(Bianca Gumina, Francesco Mauriello, Rosario Pietropaolo and Esproa, 2018)
Pd/C	Sorbitol	H2 hydrogenolysis (liquid-phase	Batch process	180°C, 5bar H_2, 24h	Conversion (60%) Selectivity: (45.4%) Ethanol (20.4) 1,2 propandiol (13.4%) 1-propanol	(Bianca Gumina, Francesco Mauriello, Rosario Pietropaolo and Esproa, 2018)

Pd/Fe_3O_4	Sorbitol	H2 hydrogenolysis (liquid-phase	Batch process	210°C, 5bar H_2, 24h	Conversion (100%) Selectivity: Ethanol (41.3%) (8.4%) 1.2 butandiol (22%) 1,2 propandiol (10%) 1-propanol	(Bianca Gumina, Francesco Mauriello, Rosario Pietropaolo and Esproa, 2018)
Pd/C	Sorbitol	H2 hydrogenolysis (liquid-phase	Batch process	210°C, 5bar H_2, 24h	Conversion (28%) Selectivity: (16.9%) Ethanol (26.1%) Ethylene glycol (11.4%) 1.2 butandiol (20.4) 1,2 propandiol (13.4%) 1-propanol	(Bianca Gumina, Francesco Mauriello, Rosario Pietropaolo and Esproa, 2018)
Pd/Fe_3O_4	Sorbitol	H2 hydrogenolysis (liquid-phase	Batch process	180°C, 5bar H_2, 24h	Conversion (91%) Selectivity: (5.5%) Xylitol (8.5%) Ethanol (7.2%) 1.2 butandiol (27.9%) 1,2 propandiol (19.5%) glycerol	(Bianca Gumina, Francesco Mauriello, Rosario Pietropaolo and Esproa, 2018)
Pd/C	sorbitol	H2 hydrogenolysis (liquid-phase	Batch process	180°C, 5bar H_2, 24h	Conversion (13.6%) Selectivity: (22%) Ethylene glycol (6%) Ethanol (12%) 1.2 butandiol (42%) 1,2 propandiol (18%) glycerol	(Bianca Gumina, Francesco Mauriello, Rosario Pietropaolo and Esproa, 2018)
Pd/Fe_3O_4	Sorbitol	H2 hydrogenolysis (liquid-phase	Batch process	150°C, 5bar H_2, 24h	Conversion (17%) Selectivity: (33%) Xylitol (8%) Ethylene glycol (12%) 1.2 butandiol (10%) 1,2 propandiol (35%) glycerol	(Bianca Gumina, Francesco Mauriello, Rosario Pietropaolo and Esproa, 2018)
Pd/C	Sorbitol	H2 hydrogenolysis (liquid-phase	Batch process	150°C, 5bar H_2, 24h	Inactive	(Bianca Gumina, Francesco Mauriello, Rosario Pietropaolo and Esproa, 2018)
Pd/(Silica-alumina)	Xylose	H2 hydrodeoxydenation	Batch process	460°C, 70 bar H_2, 5h	Conversion :(90%)	(Jackson *et al.*, 2016)

		(liquid-phase)			Selectivity :(35%) 1,6,9,13-tetraoxadispiro(4.2.4.2)tetradecane	
Pd/(Silica-alumina)	Ribose	H2 hydrodeoxydenation (liquid-phase)	Batch process	460°C, 70 bar H_2, 5h	Conversion :(93%) Selectivity :(30%) 1,6,9,13-tetraoxadispiro(4.2.4.2)tetradecane	(Jackson *et al.*, 2016)
Pd/(Silica-alumina)	L-Arabinose	H2 hydrodeoxydenation (liquid-phase)	Batch process	460°C, 70 bar H_2, 5h	Conversion :(85%) Selectivity :(32.5%) 1,6,9,13-tetraoxadispiro(4.2.4.2)tetradecane	(Jackson *et al.*, 2016)
Pd/(Silica-alumina)	Xylooligomers	H2 hydrodeoxydenation (liquid-phase)	Batch process	460°C, 70 bar H_2, 5h	Conversion :(78%) Selectivity :(32.5%) 1,6,9,13-tetraoxadispiro(4.2.4.2)tetradecane	(Jackson *et al.*, 2016)
Pd/SiO_2	Furfural	H2 hydrogenation (liquid-phase)	Batch process	100°C, 20 bar H_2, 5h	Conversion (44%) Selectivity: (10%) FA	(O'Driscoll, Leahy and Curtin, 2017)
Pd/SiO_2	Furfural	H2 hydrogenation (liquid-phase)	Batch process	100°C, 20 bar H_2, 5h	Conversion (45%) Selectivity: (8%) FA	(O'Driscoll, Leahy and Curtin, 2017)
Pd/MWCNT(multi walled carbon nano tube)	Furfural	H2 hydrogenation (liquid-phase)	Batch process	100°C, 30 bar H_2, 5h	Conversion (84.6%) Selectivity: (13.2%) FA (60.5%)THFA (14%)FDA(2-fyraldehyde diethyl acetal)	(Liu, Lou and Chen, 2018)
(Pd-Cr) /MWCNT	Furfural	H2 hydrogenation (liquid-phase)	Batch process	100°C, 30 bar H_2, 5h	Conversion (87.2%) Selectivity: (9.5%) FA (64.1%)THFA (11.8%)FDA(2-fyraldehyde diethyl acetal)	(Liu, Lou and Chen, 2018)
(Pd-Mn) /MWCNT	Furfural	H2 hydrogenation (liquid-phase)	Batch process	100°C, 30 bar H_2, 5h	Conversion (87.8%) Selectivity: (21.1%) FA (63%)THFA (10.4%)FDA(2-fyraldehyde diethyl acetal)	(Liu, Lou and Chen, 2018)

(Pd-Fe) /MWCNT	Furfural	H2 hydrogenation (liquid-phase)	Batch process	100°C, 30 bar H_2, 5h	Conversion (88.7%) Selectivity: (26.1%) FA (54.6%)THFA (8.7%)FDA(2-fyraldehyde diethyl acetal)	(Liu, Lou and Chen, 2018)
(Pd-Co) /MWCNT	Furfural	H2 hydrogenation (liquid-phase)	Batch process	100°C, 30 bar H_2, 5h	Conversion (86.8%) Selectivity: (12%) FA (70.2%)THFA (11.9%)FDA(2-fyraldehyde diethyl acetal)	(Liu, Lou and Chen, 2018)
(Pd-Ni) /MWCNT	Furfural	H2 hydrogenation (liquid-phase)	Batch process	100°C, 30 bar H_2, 5h	Conversion (92.7%) Selectivity: (2.1%) FA (78.2%)THFA (8.9%)FDA(2-fyraldehyde diethyl acetal)	(Liu, Lou and Chen, 2018)
(Pd-Ni) /MWCNT	Furfural	H2 hydrogenation (liquid-phase)	Batch process	100°C, 30 bar H_2, 5h	Conversion (92.7%) Selectivity: (2.1%) FA (78.2%)THFA (8.9%)FDA(2-fyraldehyde diethyl acetal)	(Liu, Lou and Chen, 2018)
(Pd-Ni) /AC (activated carbon)	Furfural	H2 hydrogenation (liquid-phase)	Batch process	100°C, 30 bar H_2, 5h	Conversion (55.4%) Selectivity: (25.1%) FA (42.2%)THFA (18.9%)FDA	(Liu, Lou and Chen, 2018)
(Pd-Ni) /AC (activated carbon)	Furfural	H2 hydrogenation (liquid-phase)	Batch process	100°C, 30 bar H_2, 5h	Conversion (55.4%) Selectivity: (25.1%) FA (42.2%)THFA (18.9%)FDA	(Liu, Lou and Chen, 2018)
(Pd-Ni) /H-AC (modified activated carbon)	Furfural	H2 hydrogenation (liquid-phase)	Batch process	100°C, 30 bar H_2, 5h	Conversion (41.5%) Selectivity: (13.4%) FA (56.8%)THFA (17.3%)FDA	(Liu, Lou and Chen, 2018)

(Pd-Ni) /MgO	Furfural	H2 hydrogenation (liquid-phase)	Batch process	100°C, 30 bar H_2, 5h	Conversion (46.7%) Selectivity: (30.5%) FA (24.1%)THFA (26.8%)FDA	(Liu, Lou and Chen, 2018)
(Pd-Ni) /Al_2O_3	Furfural	H2 hydrogenation (liquid-phase)	Batch process	100°C, 30 bar H_2, 5h	Conversion (53.8%) Selectivity: (34.4%) FA (45.7%)THFA (9.3%)FDA	(Liu, Lou and Chen, 2018)
(Pd-Ni) /TiO_2	Furfural	H2 hydrogenation (liquid-phase)	Batch process	100°C, 30 bar H_2, 5h	Conversion (44.3%) Selectivity: (28.3%) FA (27.8%)THFA (26.7%)FDA	(Liu, Lou and Chen, 2018)
(Pd-Ni) /ZrO_2	Furfural	H2 hydrogenation (liquid-phase)	Batch process	100°C, 30 bar H_2, 5h	Conversion (43.9%) Selectivity: (30.2%) FA (26.9%)THFA (24%)FDA	(Liu, Lou and Chen, 2018)
Pd /C-N N-doped porous carbon	Phenol	H2 hydrogenation (liquid-phase)	Batch process	110°C, 5 bar H_2, 4.5h	Conversion (98.9%) Selectivity: (96.6%) Cyclohexanone	(Hu *et al.*, 2018)
Pd/PS_{HDA} Amine functionalised carbon	1,3 butadiene	H2 hydrogenation (gas-phase)	Continuous-flow process	101°C, 10%H_2 (volume%) ,60ml/min	Conversion (40%) Selectivity: (99%) Butenes	(Castillejos *et al.*, 2018)
Pd/HTT_{HDA} Amine functionalised carbon	1,3 butadiene	H2 hydrogenation (gas-phase)	Continuous-flow process	106°C, 10%H_2 (volume%) ,60ml/min	Conversion (40%) Selectivity: (98%) Butenes	(Castillejos *et al.*, 2018)
Pd/CNT_{HDA} Amine functionalised carbon	1,3 butadiene	H2 hydrogenation (gas-phase)	Continuous-flow process	125°C, 10%H_2 (volume%) ,60ml/min	Conversion (40%) Selectivity: (100%) Butenes	(Castillejos *et al.*, 2018)
Pd/PS_{PA} Amine functionalised carbon	1,3 butadiene	H2 hydrogenation (gas-phase)	Continuous-flow process	130°C, 10%H_2 (volume%) ,60ml/min	Conversion (40%) Selectivity: (99%) Butenes	(Castillejos *et al.*, 2018)
Pd/HHT_{PA} Amine functionalised carbon	1,3 butadiene	H2 hydrogenation (gas-phase)	Continuous-flow process	29°C, 10%H_2 (volume%) ,60ml/min	Conversion (40%) Selectivity: (99%) Butenes	(Castillejos *et al.*, 2018)

Pd/CNT_{PA} Amine functionalised carbon	1,3 butadiene	H2 hydrogenation (gas-phase)	Continuous-flow process	39°C, 10%H_2 (volume%) ,60ml/min	Conversion (40%) Selectivity: (94%) Butenes	(Castillejos *et al.*, 2018)
Pd/SiO_2	Phenol	H2 hydrogenation (gas-phase)	Continuous-flow process	300°C, 1.01 bar H2 ,1.63 molar % phenol , 0.55 (g catalyst/ g phenol . hr^{-1})	Conversion (25%) Selectivity: (15%) Cyclohexanone (5%) Cyclohexanol	(Barrios *et al.*, 2018)
Pd/Nb_2O_5	Phenol	H2 hydrogenation (gas-phase)	Continuous-flow process	300°C, 1.01 bar H2 ,1.63 molar % phenol , 0.55 (g catalyst/ g phenol hr^{-1})	Conversion (55%) Selectivity: (40%) benzene	(Barrios *et al.*, 2018)
Pd/(Cellulose-C_4F_9)	Nitrobenzene	H2 hydrogenation (gas-phase)	Batch process	25°C, 1 bar H_2, 5h, H_2 balloon	Conversion (99%) Selectivity: (99%) analine	(Li, Zhang and Cai, 2018)
Pd/C	phenol	H2 hydrogenation (gas-phase)	Batch process	100°C, 10 bar H_2, 2h	Conversion (36%) Selectivity: (95%) cyclohexanone (5%) cyclohexanol	(Li *et al.*, 2018)
Pd/ Al_2O_3/monolith	2-ethyl-anthraquinone	H2 hydrogenation (liquid-phase)	Continuous-flow process	60°C, 1.01 bar ,30ml H_2/min + 50ml/ min working solution	Conversion (99.1%) Selectivity: (99.1%)2-ethyl-anthrahydroquinone	(Shi *et al.*, 2016)
GA-Pd/ZnO (Gum Acacia support)	Nitrobenzene	H2 hydrogenation (liquid-phase)	Batch process	25°C, 1.01 bar H_2, 2h	Conversion (98%) Selectivity: (98%) analine	(Supriya *et al.*, 2018)
GA-Pd/TiO_2 (Gum Acacia support)	Nitrobenzene	H2 hydrogenation (liquid-phase)	Batch process	25°C, 1.01 bar H_2, 2h	Conversion (99%) Selectivity: (99%) analine	(Supriya *et al.*, 2018)
1.3wt% Pd@MIL-101(Cr)-NH_2	Furfural	H2 hydrogenation (liquid-phase)	Batch process	40°C, 20 bar H_2, 6h	Conversion (98.9%) Selectivity: (43.3%) FA (56.7%)THFA	(Yin *et al.*, 2018)
3wt% Pd@MIL-101(Cr)-NH_2	Furfural	H2 hydrogenation (liquid-phase)	Batch process	40°C, 20 bar H_2, 6h	Conversion (99.9%) Selectivity: (0%) FA (99.9%)THFA	(Yin *et al.*, 2018)
5.4wt% Pd@MIL-101(Cr)-NH_2	Furfural	H2 hydrogenation (liquid-phase)	Batch process	40°C, 20 bar H_2, 4h	Conversion >(99.9%) Selectivity: (0.4%) FA (99.6%) THFA	(Yin *et al.*, 2018)
2.7wt% Pd@MIL-101(Cr)	Furfural	H2 hydrogenation	Batch process	40°C, 20 bar H_2, 6h	Conversion (97.7%) Selectivity: (46.8%) FA	(Yin *et al.*, 2018)

		(liquid-phase)			(53.2%)THFA	
3wt% Pd@MIL-101(Cr)-NH_2	Furfural alcohol	H2 hydrogenation (liquid-phase)	Batch process	40°C, 20 bar H_2, 2h	Conversion (100%) Selectivity: (100%)THFA	(Yin *et al.*, 2018)
Pd-Al/BC Bimorphic carbon	Cyclohexene	H2 hydrogenation (liquid-phase)	Batch process	800°C, 20 bar H_2, 1.25h	Conversion (29.7%) Selectivity: (29.7%)cyclohexane	(Cazaña *et al.*, 2018)
Pd/SiO_2	cyclohexene	H2 hydrogenation (liquid-phase)	Batch process	100°C, 20 bar H_2, 1h	Conversion (17.8%) Selectivity: (17.8%)cyclohexane	(Cazaña *et al.*, 2018)
(Pd/m-MoO_3-P_2O_5)/SiO_2	Cyclohexene	H_2 hydrogenolysis (liquid phase)	Batch process	110°C, 10 bar H_2, 2h	Conversion (100%) Selectivity: (98%)cyclohexane	(Duan *et al.*, 2017)
Pd/SiO_2	Cyclohexene	H2 hydrogenolysis (liquid phase)	Batch process	110°C, 10 bar H_2, 2h	inactive	(Duan *et al.*, 2017)
Pd-Re/C	Succinic acid	H2 hydrogenation (liquid-phase)	Batch process	180°C, 150 bar H_2, 50h	Conversion (100%) Selectivity: (49%) 1,4-Butanediol	(Minh *et al.*, 2010)
Pd-Re/C	Succinic acid	H2 hydrogenation (liquid-phase)	Batch process	160°C, 150 bar H_2, 51h	Conversion (100%) Selectivity: (62%) 1,4-Butanediol	(Minh *et al.*, 2010)
Pd-Re/C	Succinic acid	H2 hydrogenation (liquid-phase)	Batch process	160°C, 150 bar H_2, 77h	Conversion (100%) Selectivity: (66%) 1,4-Butanediol	(Minh *et al.*, 2010)
Pd/Al2O3	Levulinic acid	H2 hydrogenation (liquid-phase)	Batch process	160°C, 45 bar H_2, 6h	Conversion (31.2%) Selectivity: (94.3%) GVL	(Yan, Jarvis, *et al.*, 2013)
Pd/Al2O3	Levulinic acid	H2 hydrogenation (liquid-phase)	Batch process	160°C, 45 bar H_2, 6h	Conversion (48.7%) Selectivity: (95%) GVL	(Yan, Jarvis, *et al.*, 2013)
Pd/Al2O3	Levulinic acid	H2 hydrogenation (liquid-phase)	Batch process	160°C, 45 bar H_2, 6h	Conversion (63.2%) Selectivity: (95.2%) GVL	(Yan, Jarvis, *et al.*, 2013)
Pd-Ni/SiO_2	HMF	H2 hydrogenation (liquid-phase)	Batch process	40°C, 80 bar H_2, 2h	Conversion (99%) Selectivity: (97%) BHTF 2,5 bis-(hydroxymethyl)-tetrahydrofuran	(Nakagawa and Tomishige, 2010)

Pd-Ni/SiO_2	Furfural	H2 hydrogenation (liquid-phase)	Batch process	40°C, 80 bar H_2, 2h	Conversion (99%) Selectivity: (97%) Tetrahydrofurfuryl alcohol	(Nakagawa and Tomishige, 2010)
Pd-Ni/SiO_2	Furan	H2 hydrogenation (liquid-phase)	Batch process	40°C, 80 bar H_2, 2h	Conversion (99%) Selectivity: (98.9%) Tetrahydrofuran	(Nakagawa and Tomishige, 2010)
Pd-Ni/SiO_2	Cyclohexanone	H2 hydrogenation (liquid-phase)	Batch process	40°C, 10 bar H_2, 2h	Conversion (99%) Selectivity: (100%) cyclohexanol	(Nakagawa and Tomishige, 2010)
Pd-Ni/SiO_2	Phenol	H2 hydrogenation (liquid-phase)	Batch process	40°C, 80 bar H_2, 48h	Conversion (97%) Selectivity: (86.8%) cyclohexanol	(Nakagawa and Tomishige, 2010)
Pd-Ni/SiO_2	3-Buten-1-ol	H2 hydrogenation (liquid-phase)	Batch process	40°C, 2 bar H_2, 4h	Conversion (99%) Selectivity: (86.8%) 1-butanol	(Nakagawa and Tomishige, 2010)
Pd-Ni/SiO_2	Crotyl alcohol	H2 hydrogenation (liquid-phase)	Batch process	40°C, 2 bar H_2, 4h	Conversion (99%) Selectivity: (83.8%) 1-butanol	(Nakagawa and Tomishige, 2010)
Pd-ReMe/C	D-glucarate-6,3-lactone 1	H2 hydrogenation (liquid-phase)	Batch process	150°C, 1 bar H_2, 5h	Yield (65%) Hydroxy-(5-oxo-2,5-dihydro-furan-2-yl)-acetic acid-3-octyl ester (IUPAC name)	(Larson *et al.*, 2017)
Pd-ReMe/C	D-glucarate-6,3-lactone 1	H2 hydrogenation (liquid-phase)	Batch process	150°C, 5 bar H_2, 5h	Yield (32%) Hydroxy-(5-oxo-tetrahydro-furan-2-yl)-acetic acid ethyl ester	(Larson *et al.*, 2017)
Pd-ReMe/C	D-glucarate-6,3-lactone 1	H2 hydrogenation (liquid-phase)	Batch process	150°C, 5 bar H_2, 18h	Yield (28%) Hydroxy-(5-oxo-tetrahydro-furan-2-yl)-acetic acid ethyl ester	(Larson *et al.*, 2017)
Pd-KRe/C	D-glucarate-6,3-lactone 1	H2 hydrogenation (liquid-phase)	Batch process	150°C, 5 bar H_2, 18h	Yield:(30%) Hydroxy-(5-oxo-tetrahydro-furan-2-yl)-acetic acid ethyl ester (22%) dimethyl adipate	(Larson *et al.*, 2017)

Pd-KRe/C	D-glucarate-6,3-lactone 1	H2 hydrogenation (liquid-phase)	Batch process	150°C, 5 bar H_2, 18h	Yield:(30%) Hydroxy-(5-oxo-tetrahydro-furan-2-yl)-acetic acid ethyl ester (61%) dimethyl adipate (18%) intermediate	(Larson *et al.*, 2017)
Pd-KRe/C	D-glucarate-6,3-lactone 1	H2 hydrogenation (liquid-phase)	Batch process	150°C, 5 bar H_2, 18h 27 wt% Activated carbon additive	Yield:(30%) Hydroxy-(5-oxo-tetrahydro-furan-2-yl)-acetic acid ethyl ester (71%) dimethyl adipate	(Larson *et al.*, 2017)
Pd-KRe/C	D-glucarate-6,3-lactone 1	H2 hydrogenation (liquid-phase)	Batch process	150°C, 5 bar H_2, 18h Additives =3 mol % H3PO4, 27 wt % and activated carbon	Yield :(30%) Hydroxy-(5-oxo-tetrahydro-furan-2-yl)-acetic acid ethyl ester (88%) dimethyl adipate	(Larson *et al.*, 2017)
Pd/Starbon	Succinic acid	H2 hydrogenation (liquid-phase)	Batch process	100°C, 10 bar H_2, 24h	Conversion: (75%) Selectivity:1,4-butanediol (70%) gamma-butyrolactone (30%)	(Luque *et al.*, 2009)
Pd/Zr-P	Sorbitol	H2 hydrogenation (liquid and gas phase)	Continuous-flow process	254°C, 62 bar system P, WHSV=0.16 h^{-1}, H_2=40ml/min	Conversion:97.8% (liquid phase) Gas phase is negligible Selectivity: (5.9%) Alcohols (45.5%) Heterocyclic compounds (36.5%) Humins	(Lee, Kim and Huber, 2014)
Pd/Fe-P	Sorbitol	H2 hydrogenation (liquid and gas phase)	Continuous-flow process	254°C, 62 bar system P, WHSV=0.16 h^{-1}, H_2=40ml/min	Conversion:100% (liquid phase) Selectivity: (21.3%) Alcohols (29%) Heterocyclic compounds (24.1%) Humins	(Lee, Kim and Huber, 2014)
Pd/C	Catechol	Transfer hydrogenation (liquid-phase)	Continuous-flow process	65°C, 20 psi system P, residence time= 7 min , Sodium formate donor	Conversion:50% Selectivity:87% dihydroxycyclohexanone	(Vaccaro *et al.*, 2018)
Pd/C	Catechol	Transfer hydrogenation (liquid-phase)	Continuous-flow process	65°C, 40 psi system P, residence time= 15 min, Sodium formate donor	Conversion:90% Selectivity:85% dihydroxycyclohexanone	(Vaccaro *et al.*, 2018)

Pd/C	Catechol	Transfer hydrogenation (liquid-phase)	Continuous-flow process	90°C, 40 psi system P, residence time= 15 min , Sodium formate donor	Conversion:95% Selectivity:70% dihydroxycyclohexanone	(Vaccaro *et al.*, 2018)
Pd/C	Catechol	Transfer hydrogenation (liquid-phase)	Continuous-flow process	90°C, 40 psi system P, residence time= 15 min , Sodium formate donor	Conversion:95% Selectivity:70% dihydroxycyclohexanone	(Vaccaro *et al.*, 2018)
Pd/C	Guaiacol	Transfer hydrogenation (liquid-phase)	Continuous-flow process	90°C, 20 psi system P, residence time= 7 min , Sodium formate donor	Conversion:50% Selectivity:70% hydroxymethoxy-cyclohexanone	(Vaccaro *et al.*, 2018)
Pd/C	Guaiacol	Transfer hydrogenation (liquid-phase)	Continuous-flow process	65°C, 40 psi system P, residence time= 9 min , Sodium formate donor	Conversion:70% Selectivity:76% hydroxymethoxy-cyclohexanone	(Vaccaro *et al.*, 2018)
Pd/C	2-cresol	Transfer hydrogenation (liquid-phase)	Continuous-flow process	90°C, 40 psi system P, residence time= 15 min , Sodium formate donor	Conversion:50% Selectivity:89% hydroxymethyl-cyclohexanone	(Vaccaro *et al.*, 2018)
Pd/C	Methyl-benzyl-alcohol	hydrogenolysis (liquid-phase)	Batch process	50°C, 10 bar H_2, 1hr ethanol solvent	Conversion :(94%) Selectivity: (97.1%) Ethyl benzene	(Feng, Zhong and Dai, 2018)
Pd/C	Methyl-benzyl-alcohol	hydrogenolysis (liquid-phase)	Batch process	50°C, 10 bar H_2, 1hr ethanol solvent	Conversion :(53%) Selectivity: (92%) Ethyl benzene	(Feng, Zhong and Dai, 2018)
Pd/C	Methyl-benzyl-alcohol	hydrogenolysis 1@(liquid-phase)	Batch process	50°C, 10 bar H_2, 1hr ethanol solvent	Conversion :(68%) Selectivity: (92%) Ethyl benzene	(Feng, Zhong and Dai, 2018)